

## X-ray diffraction peaks due to misfit dislocations in heteroepitaxial structures

V. M. Kaganer,\* R. Köhler, M. Schmidbauer, and R. Opitz  
*Max-Planck-Arbeitsgruppe "Röntgenbeugung," Hausvogteiplatz 5-7, D-10117 Berlin, Germany*

B. Jenichen  
*Paul-Drude-Institut für Festkörperelektronik, Hausvogteiplatz 5-7, D-10117 Berlin, Germany*  
 (Received 28 May 1996)

The x-ray scattering from relaxed heteroepitaxial layers with the misfit dislocations randomly distributed at the interface between the layer and the substrate is analyzed theoretically and experimentally. The profiles of the x-ray-diffraction peaks and the reciprocal space maps of the intensity are measured and simulated for several heteroepitaxial structures in a wide range of dislocation densities. At large dislocation densities, the peak position is governed by the mean distortions and the peak width is due to the mean-square variations of the distortions. The peak widths calculated for uncorrelated distribution of dislocations exceed the widths of the peaks measured on the heteroepitaxial structures with large mismatch. It is shown that the spatial correlations of the dislocations reduce the peak width and explain the discrepancy. For small dislocation densities, the coherent and the diffuse components of the intensity are measured and simulated. It is shown that the position of the coherent peak does not follow the mean distortions. Satellites of the diffuse peak are observed and explained. [S0163-1829(97)02503-4]

### I. INTRODUCTION

The difference between lattice parameters of a desired epitaxial layer and that of available substrate crystals gives rise to elastic strains. These can relax by formation of surface undulations, of three-dimensional islands,<sup>1</sup> and of misfit dislocations.<sup>1,2</sup> The first two mechanisms are often restricted to the initial stages of epitaxy, while formation of misfit dislocations is a dominant mechanism at least for comparatively thick layers. The dislocation densities vary from several dislocations per sample at initial stages of the relaxation process to a dislocation per dozen lattice spacings in completely relaxed heteroepitaxial systems with large mismatch. A variety of methods are used to evaluate dislocations density and arrangement, such as etching, transmission electron microscopy,<sup>1</sup> scanning electron microscopy (electron-beam-induced current, see, e.g., Ref. 3; cathodoluminescence, see, e.g., Ref. 4), x-ray topography (see, e.g., Ref. 5) and x-ray diffractometry (see, e.g., Ref. 6). The x-ray techniques are nondestructive. X-ray topography can only be applied at comparatively low dislocation densities. X-ray diffractometry is now routinely used, in order to measure very precise values of lattice parameters and to evaluate layer thicknesses, by most laboratories which grow epitaxial layers.<sup>7</sup> When dislocation densities exceed about  $1000 \text{ cm}^{-1}$ , the strain relaxation can be calculated from the lattice-parameter measurements. Additional, hitherto unused information can be revealed from the broadening of the diffraction peaks, which is due to the nonuniformity of the strain caused by the dislocations. Experimental studies usually refer to the mosaic blocks model,<sup>8,9</sup> with the block sizes related to either the film thickness or the mean distance between threading dislocations. However, misfit dislocations located mainly at the interface between the substrate and the layer do not form block boundaries. Even when the threading dislocations densities are large, the densities of misfit dislocations in the relaxed

heterostructures are much larger, and have stronger effect on the peak widths.

The intensity of the x-ray scattering is given by the Fourier transform of the correlation function  $G(\mathbf{r}_1, \mathbf{r}_2) = \langle \exp[i\mathbf{Q} \cdot (\mathbf{u}(\mathbf{r}_1) - \mathbf{u}(\mathbf{r}_2))] \rangle$ , where  $\mathbf{u}(\mathbf{r})$  is the displacement at the site  $\mathbf{r}$  due to randomly distributed dislocations, and the average  $\langle \rangle$  is performed over their positions. The average cannot be evaluated by treating the dislocation displacements  $\mathbf{u}(\mathbf{r})$  as Gaussian random variables. To prove this statement, one simply can consider the result which the average over the Gaussian distribution would give,  $\exp\{-\frac{1}{2}\langle [\mathbf{Q} \cdot (\mathbf{u}(\mathbf{r}_1) - \mathbf{u}(\mathbf{r}_2))]^2 \rangle\}$ . The latter expression cannot be properly specified for the dislocation displacement  $\mathbf{u}(\mathbf{r})$ , defined as multivalued, or alternatively discontinuous at some arbitrary cut, function. The jump of the displacement at a cut  $\Delta\mathbf{u}(\mathbf{r}) = \mathbf{b}$ , where  $\mathbf{b}$  is the Burgers vector of the dislocation, does not cause a physical discontinuity, since the Burgers vector components are multiples of the lattice spacings, nor a problem in treating the correlation function  $G(\mathbf{r}_1, \mathbf{r}_2)$ , since the phase jump  $\mathbf{Q} \cdot \Delta\mathbf{u}(\mathbf{r}) = \mathbf{Q} \cdot \mathbf{b}$  is a multiple of  $2\pi$ , when  $\mathbf{Q}$  is a reciprocal-lattice vector.

The correct method for the calculation of the correlation function was proposed by Krivoglaz,<sup>10,11</sup> based on the Poisson statistics for uncorrelated dislocations and the Kubo cumulant expansion to take into account correlations in dislocation positions. In Appendix A, we follow Ref. 11 to derive the correlation function employed in the present study. The displacement  $\mathbf{u}(\mathbf{r})$  enters the correlation function only in the terms containing  $\exp[i\mathbf{Q} \cdot \mathbf{u}(\mathbf{r})]$ , thus excluding the problem mentioned above. Although Krivoglaz's theory was initially developed to treat the x-ray-diffraction peak profiles in metal crystals, its application to misfit dislocations is more straightforward. The assumption of parallel straight dislocations lying in a definite set of glide systems, which hardly can be justified in deformed metal crystals, is adequate to networks of misfit dislocations.

The dimensionless parameter controlling diffraction from misfit dislocations is the product  $\rho d$  of the linear dislocation density  $\rho$  and the layer thickness  $d$  (in the present study, the dislocations are assumed to be located at the interface between the layer and the substrate). This parameter varies in a very wide range: for example, the experimental results presented in Sec. V cover the range from  $\rho d \sim 0.1$  on the early stages of relaxation to  $\rho d \approx 500$  for totally relaxed layers in a heteroepitaxial system with large mismatch. In Sec. III we consider the diffraction peaks due to large dislocation densities,  $\rho d \gg 1$ , the case which is most important for the experimental studies, and allows relatively simple theoretical interpretation. In this case, the layer is strongly distorted, and only the closely spaced points  $\mathbf{r}_1$  and  $\mathbf{r}_2$  contribute to the correlation function  $G(\mathbf{r}_1, \mathbf{r}_2)$ . The coherent diffraction due to correlations between far points  $\mathbf{r}_1$  and  $\mathbf{r}_2$  is exponentially small. One can proceed from the difference of the displacements to the distortions  $\nabla \mathbf{u}(\mathbf{r})$  and represent the phase factor as  $\mathbf{Q} \cdot (\mathbf{u}(\mathbf{r}_1) - \mathbf{u}(\mathbf{r}_2)) \approx ((\mathbf{r}_1 - \mathbf{r}_2) \cdot \nabla)(\mathbf{Q} \cdot \mathbf{u}(\mathbf{r}))$ . The mean distortion  $\langle \nabla(\mathbf{Q} \cdot \mathbf{u}(\mathbf{r})) \rangle$  determines the position of the diffraction peak. Its shift with respect to that of the strained dislocation-free layer is proportional to the total Burgers vector per unit length  $\rho b$ , and coincides with the value derived considering the mean effect of the misfit dislocations.<sup>12</sup> The mean-square distortion  $\langle [\nabla(\mathbf{Q} \cdot \mathbf{u}(\mathbf{r}))]^2 \rangle$  provides the peak widths. It can be shown quite generally that the peak width is proportional to  $Qb\sqrt{\rho/d}$ , with the numerical coefficient depending on the orientations of the dislocation lines, the Burgers vectors, the diffraction vector, and on the scan direction in the reciprocal space. Analytical estimates of the coefficients and some numerical examples of the peak profiles for commonly used diffraction vectors and dislocation configurations are given in Sec. IIIB.

Networks of misfit dislocations are expected to possess correlations in the dislocation positions, due to kinetic (action of limited number of dislocation sources) and energetic (rearrangements of the dislocations to minimize elastic energy) reasons. The ideal case of randomly distributed uncorrelated dislocations can be expected only at small dislocation densities. We consider two types of correlations in the dislocation positions: short-range correlations with the correlation length  $\xi$  smaller than the layer thickness  $d$ , and long-range variations of the dislocation density. The correlations do not influence the peak position. The effect of the short-range spatial correlations on the peak width can be described by an integral parameter of the corresponding correlation function, since the dislocation distortions vary on a length scale of the order of  $d$ , large in comparison with  $\xi$ . We show in Sec. IIIC that the peak width corresponds to an effective dislocation density  $\gamma\rho$ , with the factor  $\gamma = \langle (\Delta N)^2 \rangle / N$  given by the short-range correlations. Here  $N$  is the mean number of the dislocations on an interval large in comparison with  $\xi$ , and  $\Delta N$  is the random variation of this number. If the dislocations are completely uncorrelated, as in the ideal gas of non-interacting particles, one has  $\langle (\Delta N)^2 \rangle = N$  and  $\gamma = 1$ . The correlations in dislocation positions reduce fluctuations, and the width of the diffraction peak decreases, as a result of the effective decrease of the dislocation density by a factor  $\gamma < 1$ . Calculations of the peak widths for various heteroepitaxial systems studied experimentally, performed in Sec. VI, demonstrate that the dislocations are correlated in all inves-

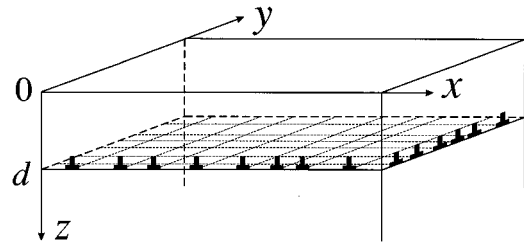


FIG. 1. Geometry of the network of the misfit dislocations in a layered heteroepitaxial system.

tigated systems with large mismatch.

When the dislocation densities vary on distances large in comparison with  $d$ , two situations are of interest. If the total density  $\rho$  varies along the interface, it can be considered as a random function  $\rho(x)$ , where  $x$  is the coordinate along the surface, with subsequent average over statistics of  $\rho(x)$ . The result is an additional broadening of the peak. In the symmetrical Bragg reflection it occurs along the diffraction vector. Another possibility is the variation of the difference  $\delta\rho = \rho_+ - \rho_-$  between the densities of two types of dislocations possessing equal misfit-releasing components  $b_x$  of the Burgers vector, but opposite tilt components  $b_z$  normal to the surface, while the total density  $\rho = \rho_+ + \rho_-$  is kept constant. Such a variation does not change the local degree of relaxation, but only causes a local tilt. Its effect on the diffraction peak is an additional broadening in the direction perpendicular to the diffraction vector.

Small dislocation densities  $\rho d \leq 1$  are considered in Sec. IV. In this case, the correlation function  $G(\mathbf{r}_1, \mathbf{r}_2)$  does not vanish in the limit of large separations  $\mathbf{r}_1 - \mathbf{r}_2 \rightarrow \infty$ . The long-range order is retained, and the diffraction spectrum contains a  $\delta$ -shaped coherent Bragg peak. The static Debye-Waller factor can be estimated as  $W \sim \rho d$ . The intensity of the Bragg peak decreases exponentially with increasing dislocation density, and practically can be observed if the mean distance between dislocations,  $\rho^{-1}$ , exceeds the layer thickness (formally the Bragg peak, albeit exponentially weak, is present for large dislocation densities also). The position of the Bragg peak is of special interest. For the reasons discussed above, the dislocation displacement  $\mathbf{u}(\mathbf{r})$  enters the expressions describing the peak position in the terms containing  $\sin(\mathbf{Q} \cdot \mathbf{u}(\mathbf{r}))$ . As  $\sin(\mathbf{Q} \cdot \mathbf{u}(\mathbf{r})) < (\mathbf{Q} \cdot \mathbf{u}(\mathbf{r}))$ , the effect of the dislocation displacements on the diffraction peak position is smaller than their effect on the mean distortions. The regions where the displacements are comparable with the Burgers vector make a large contribution to the mean distortions, but only a minor contribution to the peak shift. The position of the Bragg peak does not follow the mean distortions, contrary to the case of large dislocation densities, where they determine the position of the diffuse peak.

The geometry employed in the paper, Fig. 1, corresponds to the common geometry of the experimental studies. The misfit dislocations are supposed to lie on the interface between an epitaxial layer and a substrate at the distance  $z = d$  from the surface  $z = 0$ . Straight dislocations extend in two orthogonal directions at the interface, thus defining  $x$  and  $y$  directions in its plane, the geometry of 001-oriented crystals of zinc-blende structure with dislocations in the two orthogonal  $\langle 110 \rangle$  directions. The plane of incidence for the

triple-crystal diffraction setup is the plane  $y = \text{const}$ , as the  $\{110\}$  planes are usually chosen in the experiments. The difference between the elastic properties of the layer and substrate is neglected. We restrict ourselves with the displacement field of a straight dislocation lying parallel to the surface of the isotropic half-space.<sup>13,14</sup> The elastic anisotropy does not strongly affect the topographic images of dislocations in cubic crystals,<sup>15</sup> and its effect on the diffracted intensities is expected to be small too. Analytical expressions for the components of the displacement in an elastically isotropic half-space are presented, for the sake of completeness, in Appendix B. The misfit dislocations most commonly observed in heteroepitaxial systems are  $60^\circ$  glide dislocations. Accordingly, the dislocations with the line direction along the  $y$  axis are assumed to have Burgers vectors  $\mathbf{b} = (b_x, \pm b_y, \pm b_z)$ , where  $b_x$  is the misfit component,  $\pm b_y$  are screw components, and  $\pm b_z$  are tilt components. The densities of the dislocations differing in sign for any component of the Burgers vector are taken equal to each other, so that the possible effect of a net tilt is not considered. Densities of the dislocations extended along the  $x$  axis are taken equal to densities of the  $y$ -directed dislocations. We also consider edge (Lomer type) sessile dislocations with Burgers vectors  $\mathbf{b} = (b_x, 0, 0)$ , which are formed at large dislocation densities, as a convenient model example simplifying calculations.

## II. INTENSITY OF X-RAY SCATTERING

Our aim is to calculate the intensity of x-ray scattering from a heteroepitaxial layered structure with the dislocation network on the interface between the substrate and the layer, Fig. 1. The x-ray beams are assumed to be well collimated in the incidence plane ( $xz$  plane), while a wide acceptance window of the detector in the direction normal to this plane integrates the scattered intensity over the  $y$  component of the wave vector in infinite limits, a common geometry of a triple-crystal diffractometry experiment. In the experiments, the intensity distributions  $I(\mathbf{Q})$  are measured as the reciprocal space map of the  $\mathbf{Q} = (Q_x, Q_z)$  plane or along various directions in this plane.

The intensity  $I(\mathbf{Q})$  is concentrated at the reciprocal-lattice points. It is then convenient to consider the wave-vector deviation  $\mathbf{q} = \mathbf{Q} - \mathbf{Q}^0$  from the nearest reciprocal-lattice vector  $\mathbf{Q}^0$ . More precisely, positions of the atoms in a distorted crystal are given by the sums  $\mathbf{R}_s + \mathbf{u}(\mathbf{R}_s)$  of the position  $\mathbf{R}_s$  of the  $s$ th atom in a defect-free reference lattice and its displacement  $\mathbf{u}(\mathbf{R}_s)$  due to the lattice defects. Then the reciprocal-lattice vectors  $\mathbf{Q}^0$  are defined so that  $\mathbf{Q}^0 \mathbf{R}_s = 2\pi \times \text{integer}$ . We consider, as the reference lattice  $\{\mathbf{R}_s\}$ , the (strained) lattice of the unrelaxed layer matched to the substrate. In the kinematic approximation, the intensity scattered by the layer  $0 < z < d$  can be represented as the Fourier integral [cf. Eq. (A3)]

$$I(q_x, q_z) = \int_{-\infty}^{\infty} dx \int_0^d \int_0^d dz_s dz_{s'} e^{iq_x x + iq_z(z_s - z_{s'})} G(x, z_s, z_{s'}). \quad (1)$$

The correlations between two points  $\mathbf{R}_s(x_s, z_s)$  and  $\mathbf{R}_{s'}(x_{s'}, z_{s'})$  lying in one and the same plane  $y = \text{const}$  de-

pend on the difference  $x = x_s - x_{s'}$ , since the system is assumed uniform in the plane of the interface. The kinematical approximation is justified if the thickness of the layer is small in comparison with the extinction length. The intensity of the substrate reflection can be represented similarly to Eq. (1), by performing an integration over  $z_s$  and  $z_{s'}$  in the range  $(d, \infty)$ . An absorption factor  $\exp[-\mu(z_s + z_{s'})]$  has to be included, to ensure the convergence of the integral. Applicability of the kinematical approximation to a calculation of the intensity of the substrate peak is limited to angular deviations large in comparison with the half-width of the dynamical rocking curve. The layer and substrate peaks contain the same information about the dislocation ensemble, but the layer peak can be more easily handled both theoretically and experimentally. For that reason, we restrict ourselves to a consideration of the layer peak.

A derivation of the correlation function  $G(x, z_s, z_{s'})$ , which involves the average over statistics of the defects, was performed by Krivoglaz.<sup>10,11</sup> The main steps of the derivation are discussed in Appendix A. The correlation function is represented in the exponential form

$$G(x, z_s, z_{s'}) = \exp[-T(x, z_s, z_{s'})]. \quad (2)$$

The exponent  $T(x, z_s, z_{s'})$  is also called the correlation function below, whenever this is not confusing. Here we consider the case of uncorrelated dislocations. The exponent  $T(x, z_s, z_{s'})$  consists of two contributions,  $T = T_x + T_y$ , due to two systems of dislocations, with dislocation lines parallel to  $x$  and  $y$  axis, correspondingly. For the first system of dislocations, the summation over possible positions of the dislocations in Eq. (A8) can be replaced by the integration,  $\sum_{y'} \rightarrow a^{-1} \int dy$ , where  $a$  is the lattice spacing, and the corresponding part of the correlation function is

$$T_x(z_s, z_{s'}) = \sum_{\alpha} \rho_{\alpha} \int_{-\infty}^{\infty} dy \{1 - e^{i\mathbf{Q} \cdot [\mathbf{u}_{\alpha}(y, z_s) - \mathbf{u}_{\alpha}(y, z_{s'})]}\}. \quad (3)$$

Here  $\rho_{\alpha} = c_{\alpha}/a$  is the linear density of dislocations, the subscript  $\alpha$  denotes different types of Burgers vectors,  $c_{\alpha}$  is the number density of dislocations introduced in Appendix A, and  $\mathbf{u}_{\alpha}(y, z)$  is the displacement at the point  $(y, z)$  due to a dislocation of type  $\alpha$  at the origin. This part of the correlation function does not depend on  $x$ , since the displacement fields of the dislocations lying parallel to the incidence plane  $(x, z)$  are  $x$  independent. The contribution due to dislocations perpendicular to the incidence plane reads

$$T_y(x, z_s, z_{s'}) = \sum_{\alpha} \rho_{\alpha} \int_{-\infty}^{\infty} dx' \times \{1 - e^{i\mathbf{Q} \cdot [\mathbf{u}_{\alpha}(x', z_s) - \mathbf{u}_{\alpha}(x', z_{s'})]}\}, \quad (4)$$

and depends on  $x$ .

The symmetries of  $T_x$  and  $T_y$  with respect to their arguments directly follow from Eqs. (3) and (4):  $T_x(z_2, z_1) = T_x^*(z_1, z_2)$  and  $T_y(-x, z_2, z_1) = T_y^*(x, z_1, z_2)$ , where the asterisk denotes complex conjugation. Then intensity (1) can be represented as an integral of a real function,

$$I(q_x, q_z) = 2 \int_0^\infty dx \int_0^d \int_0^d dz_s dz_{s'} e^{-T'(x, z_s, z_{s'})} \times \cos[q_x x + q_z(z_s - z_{s'}) - T''(x, z_s, z_{s'})]. \quad (5)$$

Here  $T'$  and  $T''$  are real and imaginary parts, respectively, of the correlation function  $T = T_x + T_y$ .

Some further symmetry of the correlation function can be found in the important particular case of symmetrical Bragg reflection,  $\mathbf{Q} = (0, 0, Q_z)$ , with equal densities of dislocations possessing opposite  $z$  components of the Burgers vectors. In this case the symmetry properties of the displacement fields given in Appendix B can be exploited: for the displacement field  $\mathbf{u}^{(x)}$  due to the  $x$  component of the Burgers vector, one has  $u_x^{(x)}(-x, z) = -u_x^{(x)}(x, z)$  and  $u_z^{(x)}(-x, z) = u_z^{(x)}(x, z)$ , while for the displacements  $\mathbf{u}^{(z)}$  due to the  $z$  component gives  $u_x^{(z)}(-x, z) = u_x^{(z)}(x, z)$  and  $u_z^{(z)}(-x, z) = -u_z^{(z)}(x, z)$ . Then, in addition one has  $T(-x, z_1, z_2) = T(x, z_1, z_2)$ , and Eq. (5) reduces to

$$I(q_x, q_z) = 2 \int_0^\infty dx \cos q_x x \int_0^d \int_0^d dz_s dz_{s'} e^{-T'(x, z_s, z_{s'})} \times \cos[q_z(z_s - z_{s'}) - T''(x, z_s, z_{s'})]. \quad (6)$$

### III. DIFFRACTION PEAKS AT LARGE DISLOCATION DENSITIES

#### A. Positions of the peaks

In this section we consider large densities of the misfit dislocations,  $\rho d \gg 1$ . In this case, the exponents  $T_x$  and  $T_y$  contain large prefactors. When the distance between the points  $\mathbf{R}_s$  and  $\mathbf{R}_{s'}$  is not small, and the integrals in Eqs. (3) and (4) are of the order of  $d$ , one can estimate  $T \sim \rho d$ , and the contribution to the correlation function  $G = \exp(-T)$  is exponentially small. Thus the correlations between closely spaced points  $\mathbf{R}_s$  and  $\mathbf{R}_{s'}$  are of interest only. The differences of displacements in Eqs. (3) and (4) can be expanded over small quantities  $x$  and  $\zeta = z_s - z_{s'}$ , retaining the linear terms:

$$\mathbf{Q} \cdot \mathbf{u}_\alpha(x', z_s) - \mathbf{Q} \cdot \mathbf{u}_\alpha(x' - x, z_{s'}) \approx_x \frac{\partial \mathbf{Q} \cdot \mathbf{u}_\alpha(x', z_s)}{\partial x'} + \zeta \frac{\partial \mathbf{Q} \cdot \mathbf{u}_\alpha(x', z_s)}{\partial z_s}. \quad (7)$$

Then the exponential functions in Eqs. (3) and (4) can also be expanded. The first term of the expansion is imaginary and linear with respect to  $x$  and  $\zeta$ ,

$$T''(x, z_s, z_{s'}) = q_{0x}x + q_{0z}\zeta, \quad (8)$$

where

$$q_{0x} = - \sum_\alpha \rho_\alpha \int_{-\infty}^\infty dx \frac{\partial \mathbf{Q} \cdot \mathbf{u}_\alpha(x, z)}{\partial x}, \quad (9)$$

$$q_{0z} = - 2 \sum_\alpha \rho_\alpha \int_{-\infty}^\infty dx \frac{\partial \mathbf{Q} \cdot \mathbf{u}_\alpha(x, z)}{\partial z}$$

are proportional to the mean distortions due to uniformly distributed dislocations. The factor 2 in the expression for  $q_{0z}$  is due to the contribution of dislocations both parallel

and perpendicular to the incidence plane, with the integration variable  $y$  in Eq. (3) is substituted for by  $x$ . Only dislocations perpendicular to the incidence plane contribute to  $q_{0x}$ .

Integrals (9), with the displacements due to dislocations lying parallel to the surface of an isotropic half-space given in Appendix B, can be calculated analytically. The result is

$$q_{0x} = \rho Q_x b_x, \quad q_{0z} = - \frac{2\nu}{1-\nu} \rho Q_z b_x, \quad (10)$$

where  $\nu$  is the Poisson ratio and  $\rho = \sum_\alpha \rho_\alpha$  is total density of the dislocations lying parallel or perpendicular to the incidence plane. The mean distortions are constant, despite the fact that the integrands are  $z$  dependent, and depend only on the total  $x$  component of the Burgers vectors per unit length  $\rho b_x$ , since the densities of the dislocations with  $\pm b_z$  are taken equal to each other, and the integrals are linear over  $\mathbf{b}$ . On Fourier transformation (1), the phase factor given by Eq. (8) yields a shift of the diffraction peak by  $\mathbf{q}_0 = (q_{0x}, q_{0z})$ . This value coincides with the well-known result of Chu *et al.*,<sup>12</sup> who treated a net effect of the dislocations without considering their individual displacements. We note that Chu *et al.* did not argue, why the position of the diffraction maximum follows the mean distortions. In the framework of our considerations, this is a result of the expansion (7), which implies that only the displacements at closely spaced points are correlated. This assumption is justified for large densities of dislocations,  $\rho d \gg 1$ , but is not valid for the small dislocation densities considered in Sec. IV.

#### B. Shapes of the peaks

We begin the analysis of the peak shape with the particular case of a symmetrical Bragg reflection  $\mathbf{Q} = (0, 0, Q_z)$ , which is of primary experimental interest and also allows us to make calculations transparent by considering a simplest situation. The real part of the correlation function  $T'$  can be received by applying approximation (7) and expanding the exponential functions in Eqs. (4) and (5) up to second order over  $x$  and  $\zeta$ ,

$$T'(x, z_s, z_{s'}) = w_x(z_s)x^2 + w_z(z_s)\zeta^2. \quad (11)$$

Then the intensity (1) can be evaluated by extending the integration over  $\zeta$  to infinite limits, due to the fast decay of the integrand. Integral (1) with the Gaussian function  $\exp(-T)$  gives

$$I(q_x, q_z) = \pi \int_0^d \frac{dz}{\sqrt{w_x w_z}} \exp \left[ - \frac{(q_x - q_{x0})^2}{4w_x} - \frac{(q_z - q_{z0})^2}{4w_z} \right]. \quad (12)$$

To evaluate the coefficients  $w_x(z)$  and  $w_z(z)$ , let us separate the displacements due to different components of the Burgers vectors:  $\mathbf{u} = \mathbf{u}^{(x)} + \mathbf{u}^{(y)} + \mathbf{u}^{(z)}$ . We consider dislocations perpendicular to the incidence plane with the Burgers vectors  $\mathbf{b} = (b_x, \pm b_y, \pm b_z)$  and those parallel to it with  $\mathbf{b} = (\pm b_y, b_x, \pm b_z)$ . The component  $b_x$ , equal for dislocations of all types, releases the mismatch. Other components take opposite values with equal probability, giving a net tilt equal to zero. The consideration thus includes the edge and

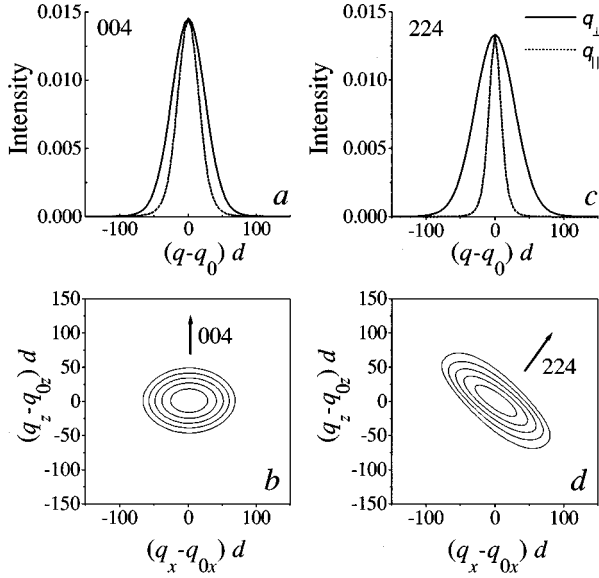


FIG. 2. Intensity distributions for edge dislocations calculated with Eqs. (12) and (16) for 004 and 224 reflections: (a) and (c) scans along and perpendicular to the diffraction vectors; and (b) and (d) the reciprocal space maps. The intensity changes between isointensity contours by a factor of 2.

the  $60^\circ$  dislocations with Burgers vectors  $\frac{1}{2}\langle 110 \rangle$ . The expansion of Eqs. (3) and (4) gives

$$w_x(z) = \frac{1}{2} \rho Q_z^2 \int_{-\infty}^{\infty} dx [u_{z,x}^{(x)2} + u_{z,x}^{(z)2}], \quad (13)$$

$$w_z(z) = \rho Q_z^2 \int_{-\infty}^{\infty} dx [u_{z,z}^{(x)2} + u_{z,z}^{(z)2}].$$

Here  $u_{i,j} = \partial u_i / \partial x_j$  and  $i, j = x, z$ . The integration variable was changed from  $y$  to  $x$  when calculating  $T'_x$ . The coefficients at  $w_x$  and  $w_z$  differ by a factor 2, which is due to contribution of dislocations of the two systems to  $w_z$ , while only dislocations perpendicular to the diffraction plane contribute to  $w_x$ . The screw component  $\mathbf{u}^{(y)}$  does not contribute to the symmetrical Bragg reflection. When the edge dislocations with the Burgers vectors in the layer plane are considered, only  $\mathbf{u}^{(x)}$  is nonzero.

The intensity distributions calculated by numerical integration of Eq. (12) for the symmetrical 004 reflection are presented in Figs. 2(a) and 2(b) and Fig. 3(a) and 3(b) for edge and  $60^\circ$  dislocations, respectively. The anisotropic intensity distributions are extended perpendicularly to the diffraction vector (along  $q_x$ ). The peak aspect ratio  $\Delta q_z / \Delta q_x$  is 0.68 for edge dislocations, and 0.30 for  $60^\circ$  dislocations.

Intensity distribution (12) involves anisotropic Gaussians of different widths, since the factors  $w_x$  and  $w_z$  depend on  $z$ . The smooth functions  $w_x(z)$  and  $w_z(z)$  increase when  $z$  tends to  $d$ , while the contribution to the integral decreases. The integral (12) can be estimated by taking  $w_x$  and  $w_z$  at  $z=0$ , which gives  $I(q_x, q_z) \sim \exp[-(q_x - q_{x0})^2 / 4w_x(0) - (q_z - q_{z0})^2 / 4w_z(0)]$ . In this estimate, the peak is an anisotropic Gaussian with the longitudinal to transverse peak width ratio  $\Delta q_z / \Delta q_x = \sqrt{w_z(0) / w_x(0)}$ . Integrals (13) can be

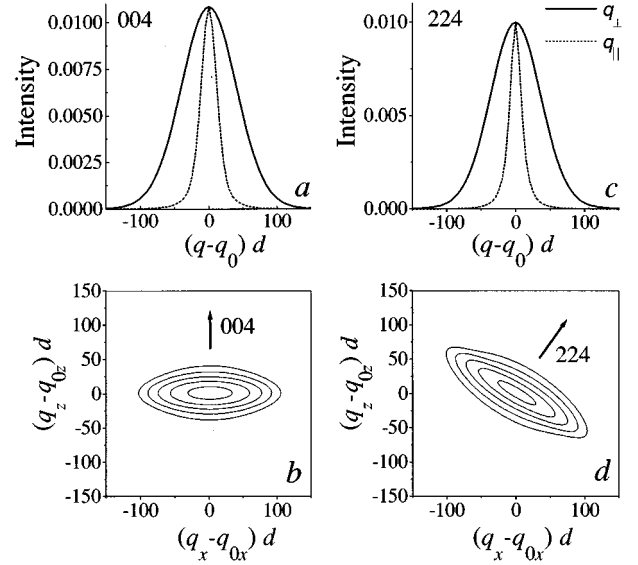


FIG. 3. Intensity distributions for  $60^\circ$  dislocations calculated with Eqs. (12) and (16) for 004 and 224 reflections: (a) and (c) scans along and perpendicular to the diffraction vectors, and (b) and (d) the reciprocal space maps. The intensity changes between isointensity contours by a factor of 2.

evaluated analytically at  $z=0$ . For edge dislocations, one has  $w_x(0) = \rho Q_z^2 b_x^2 / (8\pi d)$  and  $w_z(0) = [\nu / (1 - \nu)]^2 \rho Q_z^2 b_z^2 / (4\pi d)$ . The peak aspect ratio  $\Delta q_z / \Delta q_x = \sqrt{2\nu / (1 - \nu)}$  depends on the Poisson ratio  $\nu$  only. For  $\nu=0.3$ , one has  $\Delta q_z / \Delta q_x \approx 0.6$ . When several types of dislocations are present, calculations give  $w_x(0) = \rho Q_z^2 (b_x^2 + 5b_z^2) / (8\pi d)$  and  $w_z(0) = \rho Q_z^2 [\nu / (1 - \nu)]^2 (b_x^2 + b_z^2) / (4\pi d)$ . In particular, the  $60^\circ$  dislocations give the peak aspect ratio  $\Delta q_z / \Delta q_x = \sqrt{6/11} \nu / (1 - \nu) \approx 0.27$ , in agreement with the results of the numerical integration.

The calculations above show that the peak width of an epitaxial layer is dominated by the nonuniformity of distortions in the near-surface part of the layer. In particular, a thin nonrelaxed layer grown on the top of a relaxed buffer layer shows the same nonuniformity of distortions as the buffer layer. It also follows from the estimate above that the peak widths  $\Delta q_{x,z}$  are proportional to  $Q_z b_x \sqrt{\rho} / d$ . When the dislocation density varies, the plots of Figs. 2 and 3 are scaled as  $\sqrt{\rho}$ . The longitudinal and transverse peak widths for  $60^\circ$  dislocations found by numerical integration of Eq. (12) are plotted in Fig. 4 as functions of the dislocation density. The plotted dependencies can be written as  $\Delta q_x = 21.3 \sqrt{\rho} / d$  and  $\Delta q_z = 6.2 \sqrt{\rho} / d$ . The estimates presented above give an accuracy of about 10%.

Expansion (7) is applicable when  $x, \zeta \ll d$ . With the estimate  $w_x, w_z \sim (\rho/d)(Qb)^2$  received above, the real part of the correlation function is  $T' \sim (\rho/d)(Qb)^2 x^2$  (plus the similar term proportional to  $\zeta^2$ ). The behavior of the correlation function is of interest in the range  $T' \leq 1$ , since the contribution of large  $T'$  to Eq. (2) is exponentially small. Thus, the actual range of distances is  $x/d \leq (Qb \sqrt{\rho d})^{-1}$ . When the requirement  $\rho d \gg 1$  imposed in this section is satisfied, this range is small,  $x \ll d$ , thus ensuring the applicability of the approximations made above. A comparison of approximation (12) with numerical integration of the exact expression (1)

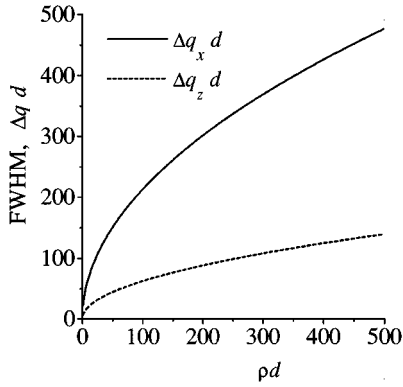


FIG. 4. Longitudinal and transverse full width at half maximum (FWHM) of the calculated diffraction peaks for  $60^\circ$  dislocations with Burgers vectors  $\frac{1}{2}(110)$  in the symmetrical 004 Bragg reflection.

for dislocation density  $\rho d = 20$  (not presented) gives a difference of less than 1%, comparable to the accuracy of the calculations. When the dislocation density is small,  $\rho d \leq 1$ , the approximation made in the present section cannot be applied. This case is considered in Sec. IV.

It is worth noting that the results presented above for misfit dislocations distributed in the plane of the interface differ from the results received by Krivoglaz<sup>11</sup> for straight dislocations uniformly distributed parallel to each other in a bulk crystal. The dislocation distortions behave as  $\nabla \mathbf{u} \sim 1/r$  in the infinite solid. The integrals similar to Eq. (13) in the bulk crystal,  $\int d^2r (\nabla \mathbf{u})^2$ , diverge proportional to  $\ln L$ , where  $L$  is the system size. As a result, the peak width logarithmically depends on the system size. One-dimensional integrals of the present problem  $\int dx (\nabla \mathbf{u})^2$ , with  $\nabla \mathbf{u}$  decreasing as  $1/x$  or faster, converge, and the peak width is size independent.

Let us proceed to a general case of an asymmetric reflection  $\mathbf{Q} = (Q_x, 0, Q_z)$ . Using expansion (7), one receives

$$T'(x, z_s, z_{s'}) = w_{xx}(z_s)x^2 + 2w_{xz}(z_s)x\zeta + w_{zz}(z_s)\zeta^2. \quad (14)$$

To evaluate the coefficients, one takes into account that  $u_x^{(x)}(x, z)$  and  $u_z^{(z)}(x, z)$  are odd functions of  $x$ , while  $u_x^{(z)}(x, z)$  and  $u_z^{(x)}(x, z)$  are even functions of  $x$ . Then one has

$$\begin{aligned} w_{xx}(z) &= \frac{\rho}{2} \sum_{\sigma=x,z} \int_{-\infty}^{\infty} dx (Q_x^2 u_{x,x}^{(\sigma)2} + Q_z^2 u_{z,x}^{(\sigma)2}), \\ w_{xz}(z) &= \frac{\rho}{2} Q_x Q_z \sum_{\sigma=x,z} \int_{-\infty}^{\infty} dx (u_{x,x}^{(\sigma)} u_{z,z}^{(\sigma)} + u_{x,z}^{(\sigma)} u_{z,x}^{(\sigma)}), \\ w_{zz}(z) &= \frac{\rho}{2} \left\{ \sum_{\sigma=x,z} \int_{-\infty}^{\infty} dx (Q_x^2 u_{x,x}^{(\sigma)2} + 2Q_z^2 u_{z,z}^{(\sigma)2}) \right. \\ &\quad \left. + \int_{-\infty}^{\infty} dx Q_x^2 u_{x,z}^{(y)2} \right\}. \end{aligned} \quad (15)$$

For edge dislocations, only the  $u^{(x)}$  component of the displacements contribute to Eq. (15).

Performing the Fourier transformation (1) with the real part of the correlation function (14) and the imaginary part (8), one has the intensity

$$I(q_x, q_z) = \pi \int_0^d \frac{dz}{\sqrt{\det \hat{w}}} \exp\left[-\frac{1}{4} w_{ij}^{-1}(\mathbf{q} - \mathbf{q}_0)_i (\mathbf{q} - \mathbf{q}_0)_j\right], \quad (16)$$

where  $\hat{w}$  is a  $2 \times 2$  symmetrical matrix with the elements  $w_{ij}$  given by Eq. (15), and  $i, j = x, z$ , and  $w_{ij}^{-1}$  are elements of the reciprocal matrix  $\hat{w}^{-1}$ . The intensity distributions calculated by numerical integration of Eq. (16) for the asymmetrical 224 reflection are presented in Figs. 2(c) and 2(d) and Fig. 3(c) and 3(d). The anisotropic intensity distributions are extended perpendicularly to the diffraction vector.

To estimate integral (16), one can take, as above, the smooth functions  $w_{ij}(z)$  at  $z=0$ . Analytical integration of Eq. (15) for the edge dislocations yields  $w_{xx}(0) = \rho (Q_x^2 + Q_z^2) b_x^2 / (8\pi d)$ ,  $w_{xz}(0) = -(1-\nu)\rho Q_x Q_z b_x^2 / (8\pi d)$ , and  $w_{zz}(0) = \rho(Q_x^2 + 2[\nu/(1-\nu)]^2 Q_z^2) b_x^2 / (8\pi d)$ . The orientation of the anisotropic Gaussian distribution of the intensity follows orientation of the main axes of the tensor  $\hat{w}^{-1}$ . The angle  $\varphi$  between  $z$  axis and the minor axis of the tensor is given by  $\tan 2\varphi = 2w_{xz}/(w_{zz} - w_{xx})$ . Calculating this angle for the 224 reflection, one receives  $\varphi = 36^\circ$ . The angle between the diffraction vector and  $z$  axis is  $\arctan(Q_x/Q_z) = 35^\circ$ , i.e., the intensity distribution is extended almost perpendicularly to the diffraction vector. The iso-intensity map, Fig. 2(d), confirms this conclusion. It is worth noting, however, that there is no symmetry-related restriction for the orientation of the intensity distribution with respect to the diffraction vector. The two directions occur close to each other for commonly used reflections. Orientations of the intensity distributions with respect to the diffraction vector are slightly different for edge and  $60^\circ$  dislocations, cf. Figs. 2(d) and 3(d).

### C. Spatial correlations of dislocations

The considerations above assume that dislocations take their positions independently from each other. One can expect, however, that the misfit dislocations are correlated due to kinetic and energetic reasons: the dislocations are created by a limited number of the sources and then redistribute to minimize the elastic energy. Regular arrays of the misfit dislocations are reported for large densities of the dislocations. The spatial correlations of the dislocations can be taken into account in evaluation of the x-ray correlation function  $G(x, z_s, z_{s'})$ , as discussed in the Appendix A. However, the correlation functions are not known, and in addition calculations become complicated even if only pair correlations are involved.

For large dislocation densities, when the mean distance between dislocations is much smaller than the layer thickness  $d$ , one can expect that the correlation length of the spatial correlations is also small in comparison with  $d$ . Then the effect of spatial correlations can be taken into account rather easily, since the characteristic length of the correlation function  $\varepsilon_{\alpha\alpha'}(\mathbf{R}_i - \mathbf{R}_{i'})$  entering Eq. (A12) is much smaller than  $d$ , while the factors  $\Phi_{i\alpha}$  vary on distances comparable with  $d$  and can be kept constant during summation of the correlation function. Equation (A12) simplifies to

$$T(\mathbf{R}_s, \mathbf{R}_{s'}) = \sum_{i\alpha} c_\alpha \Phi_{i\alpha} - \frac{1}{2} \sum_{\alpha\alpha'} \varepsilon_{\alpha\alpha'} \sum_i \Phi_{i\alpha} \Phi_{i\alpha'}, \quad (17)$$

where  $\epsilon_{\alpha\alpha'} = \sum_i \epsilon_{\alpha\alpha'}(\mathbf{R}_i)$  are constant factors describing the correlations, and  $\Phi_{i\alpha} = \exp[i\mathbf{Q} \cdot (\mathbf{u}_{s'i\alpha} - \mathbf{u}_{s't\alpha})] - 1$  are the same factors as in Eqs. (3) and (4). The first term of Eq. (17) describes uncorrelated dislocations, and the second term is due to spatial correlations of the dislocations. Making use of approximation (7), one expands  $\Phi_{i\alpha}$  in the first term of Eq. (17) up to the terms of the second order over  $x$  and  $\zeta$ . In the second term of Eq. (17) the expansion of  $\Phi_{i\alpha}$  can be restricted, with the same accuracy, with the terms linear over  $x$  and  $\zeta$ . The higher-order correlation functions entering Eq. (A11) can be neglected, since they give terms of higher order over  $x$  and  $\zeta$ .

Let us first consider the case of dislocations with only one type of the Burgers vectors, the edge dislocations. Correlations between dislocations either parallel or perpendicular to the incidence plane are described by a single correlation parameter  $\epsilon = \sum_i \epsilon(\mathbf{R}_i)$ , and the two systems of dislocations are assumed to be uncorrelated with each other. The spatial correlations of the dislocations do not contribute to the imaginary part  $T''$  of the x-ray correlation function. Thus, the diffraction peak due to spatially correlated dislocations remains in the same position due to uncorrelated dislocations. In the real part  $T'$  of the x-ray correlation function, the second term of Eq. (17) contributes by changing the number density of dislocations  $c$  by  $c + \epsilon$ . Equations (14)–(16) remain applicable after multiplying the dislocation density  $\rho$  by a factor  $\gamma = 1 + c^{-1}\epsilon$ . Thus the peak width is influenced by the correlations by replacing the dislocation density  $\rho$  by an effective density  $\gamma\rho$ . As shown in Appendix A, the correlation parameter  $\gamma$  can be quite generally related to fluctuations of the number of dislocations:  $\gamma = \langle (\Delta N)^2 \rangle / N$ , where  $N$  is the mean number of dislocations in some interval, and  $\Delta N$  is a random variation of this quantity. Positionally uncorrelated dislocations can be considered as a gas of noninteracting particles, which gives  $\langle (\Delta N)^2 \rangle = N$ , and thus  $\gamma = 1$ . The correlated dislocations can be treated similarly to a liquid, where distances between particles deviate only slightly from the mean distance, and fluctuations of the number of particles are smaller than in the gas,  $\langle (\Delta N)^2 \rangle < N$ . Then the correlation parameter  $\gamma < 1$  and the diffraction peak is narrower than at the same density of uncorrelated dislocations. In Secs. V and VI we compare the experimental data for several heteroepitaxial systems with calculations in the framework of the present approach, and find that in the relaxed systems possessing large mismatch, the observed peaks are considerably narrower than the peaks calculated for uncorrelated dislocations, so that the correlation parameter  $\gamma \ll 1$ .

For several types of dislocations with the Burgers vectors  $\mathbf{b} = (b_x, \pm b_y, \pm b_z)$ , one can introduce correlation factors  $\epsilon_{11}$  for correlations between dislocations with one and the same Burgers vector, and  $\epsilon_{12}$  for dislocations with different Burgers vectors. Then, for a symmetrical Bragg reflection, Eqs. (13) are replaced by

$$\begin{aligned} w_x(z) &= \frac{1}{2} \rho Q_z^2 \int_{-\infty}^{\infty} dx [\gamma_1 u_{z,x}^{(x)2} + \gamma_2 u_{z,x}^{(z)2}], \\ w_z(z) &= \rho Q_z^2 \int_{-\infty}^{\infty} dx [\gamma_1 u_{z,z}^{(x)2} + \gamma_2 u_{z,z}^{(z)2}], \end{aligned} \quad (18)$$

where  $\gamma_1 = 1 + c_1^{-1}(\epsilon_{11} + \epsilon_{12})$ ,  $\gamma_2 = 1 + c_1^{-1}(\epsilon_{11} - \epsilon_{12})$ , and  $c_1$  is the number density of dislocations of each type. Two correlation parameters  $\gamma_1$  and  $\gamma_2$  can be found in the x-ray-diffraction experiment by measuring the peak widths in directions along and perpendicular to the diffraction vector. When the correlations between dislocations of different types are absent, i.e.,  $\epsilon_{12} = 0$ , one can introduce, as above, a single factor  $\gamma = \gamma_1 = \gamma_2$  related to the mean-square fluctuations of number of the dislocations.

The dislocation distribution can have, in addition to the spatial correlations on the length scale small in comparison with the layer thickness  $d$ , nonuniformities with a characteristic length large in comparison with  $d$ . This long-range nonuniformity can be taken into account by considering a varying dislocation density  $\rho = \rho(x)$ . The main effect is due to local variations of the peak position, rather than variations of the peak width. Including a random variation  $\delta\rho(x)$  of the dislocation density in Eq. (9) and treating it as a Gaussian random variable, one has an additional contribution

$$\delta T' = \frac{1}{2} \langle (\delta\rho/\rho)^2 \rangle (q_{0x}x + q_{0z}\zeta)^2 \quad (19)$$

to the correlation function (11) and an additional broadening of the diffraction peaks. In the symmetrical Bragg reflection, in particular, the peak broadens in the  $q_z$  direction.

Another possibility is a variation  $\delta\rho = \rho_+ - \rho_-$  of the relative densities  $\rho_{\pm}$  of the two types of dislocations with Burgers vectors  $(b_x, b_y, \pm b_z)$  with the same misfit component  $b_x$  and the opposite tilt components  $\pm b_z$ , which is energetically less costly, since it does not change the local degree of relaxation. Keeping the total density  $\rho = \rho_+ + \rho_-$  constant, one obtains an additional contribution to Eq. (8):

$$\delta\rho \left( x \int_{-\infty}^{\infty} dx \frac{\partial Q_z u_z^{(z)}}{\partial x} + \zeta \int_{-\infty}^{\infty} dx \frac{\partial Q_x u_x^{(z)}}{\partial z} \right). \quad (20)$$

The integrals of Eq. (20), calculated with the displacements given in Appendix B, are equal to  $-Q_z b_z$  and  $Q_x b_z$ , respectively. Averaging over a Gaussian distribution of  $\delta\rho(x)$ , one finds the contribution to the correlation function,

$$\delta T' = \frac{1}{2} \langle (\delta\rho/\rho)^2 \rangle (Q_z x - Q_x \zeta)^2 b_z^2, \quad (21)$$

which gives rise to an additional broadening of the diffraction peak in the direction orthogonal to the diffraction vector  $\mathbf{Q}$ , due to local variations of the tilt.

#### IV. DIFFRACTION PEAKS AT SMALL DENSITIES OF DISLOCATIONS

The approximations of Sec. III are developed for large densities of dislocations. For small dislocation densities  $\rho d \lesssim 1$ , a general analysis based on the equations of Sec. II has to be performed. The presence or absence of the coherently scattered wave depends on the long-range limit of the correlation function.<sup>11</sup> Let us consider the limit of the correlation function  $T(x, z_s, z_{s'})$  on large separations,  $T_{\infty}(z_s, z_{s'}) = \lim_{x \rightarrow \infty} T(x, z_s, z_{s'})$ . The contribution due to dislocations parallel to the incidence plane  $T_x(z_s, z_{s'})$  does not depend on  $x$ . The limit  $T_{\infty y}$  due to dislocations perpendicular to the incidence plane is finite, as will be shown below. Then the intensity  $I(q_x, q_z)$  contains a term propor-

tional to the delta function  $\delta(q_x)$ , which reflects presence of the long-range order in the layer and can be referred to as the coherent intensity. One can present the intensity as

$$I(q_x, q_z) = 2\pi\delta(q_x)I_{\text{coh}}(q_z) + I_{\text{diff}}(q_x, q_z), \quad (22)$$

where

$$I_{\text{coh}}(q_z) = \int_0^d \int_0^d dz_s dz_{s'} e^{iq_z(z_s - z_{s'})} e^{-T_\infty(z_s, z_{s'})} \quad (23)$$

is the coherent intensity. In a dislocation-free layered system  $T=0$ , one has the well-known result  $I_{\text{coh}}(q_z) = 4q_z^{-2} \sin^2(q_z d/2)$ . The remaining part of the intensity, which does not exhibit singularities,

$$I_{\text{diff}}(q_x, q_z) = \int_{-\infty}^{\infty} dx \int_0^d \int_0^d dz_s dz_{s'} e^{iq_x x + iq_z(z_s - z_{s'})} \times [e^{-T(x, z_s, z_{s'})} - e^{-T_\infty(z_s, z_{s'})}], \quad (24)$$

is the diffuse intensity.

The calculations involve several infinity limits: the correlation function  $T(x, z_s, z_{s'})$  is a result of the integration (4) in the infinite limits, while its limit at  $x \rightarrow \infty$  is applied in the integral (1) also taken in the infinite limits. The hierarchy can be imposed as follows. The integral (4) for the correlation function  $T(x, z_s, z_{s'})$  is taken, as is shown in Appendix A [Eq. (A8)], over all possible positions of the dislocations in the sample,  $x \in (-L_s, L_s)$ , where  $2L_s \times 2L_s$  is the lateral sample size. The Fourier transformation (1) corresponds to a summation over the area illuminated by the x rays, cf. Eq. (A3),  $x \in (-L_i, L_i)$ , where  $2L_i \times 2L_i$  is the size of the illuminated area. We take, as it is usually realized experimentally,  $L_i \ll L_s$ . The limit  $x \rightarrow \infty$  of the correlation function  $T(x, z_s, z_{s'})$  implies  $d \ll x \sim L_i \ll L_s$ . Therefore, one can consider the correlation function  $T(x, z_s, z_{s'})$  as a result of the integration (4) in the infinite limits for a finite  $x$ , and proceed to the limit  $x \rightarrow \infty$  on the next stage. The delta function  $\delta(q_x)$  in Eq. (22) represents a peak with the height proportional to  $L_i$ , and a half-width of the order of  $L_i^{-1}$ .

To find the limit  $T_{\infty y}$ , one takes into account that the dislocation displacements  $\mathbf{u}_\alpha(x', z)$  tend to zero at large  $x'$ , and either one or the other of the two displacements entering Eq. (4) is small during integration at infinitely large separation  $x$ . The real part  $T'_{\infty y}$  can be represented as a sum  $T'_{\infty y}(z_s, z_{s'}) = W(z_s) + W(z_{s'})$ , where

$$W(z) = \sum_\alpha \rho_\alpha \int_{-\infty}^{\infty} dx \{1 - \cos(\mathbf{Q} \cdot \mathbf{u}_\alpha(x, z))\} \quad (25)$$

is a static Debye-Waller factor due to dislocations perpendicular to the incidence plane. The contribution  $T'_x(z_s, z_{s'})$  to the coherent peak due to dislocations parallel to the incidence plane cannot be represented in this way. When  $x \rightarrow \infty$ , the dislocation displacements  $\mathbf{u}_\alpha$  decrease as  $1/x$  or faster, the cosine term in Eq. (25) can be expanded in power series and the integral  $\int (\mathbf{Q} \cdot \mathbf{u})^2 dx$  converges, thus ensuring that the Debye-Waller factor  $W(z)$  is finite. This is dissimilar to the dislocations uniformly distributed in a bulk crystal, where the two-dimensional integral  $\int (\mathbf{Q} \cdot \mathbf{u})^2 d^2 r$  diverges at  $r \rightarrow \infty$ , the Debye-Waller factor is infinite, and the true Bragg

peak is absent.<sup>11</sup> To estimate  $T'_x$  and  $W$ , one takes into account that the terms in the wavy brackets of Eqs. (3) and (25) are of the order of unity for  $|x| \lesssim d$ , and decrease for larger  $x$  fast enough. Then the estimate is  $W, T'_x \sim \rho d$ . The coherent intensity is exponentially small when the dislocation density is large,  $\rho d \gg 1$ . For that reason the coherent intensity was not taken into account in Sec. III.

In a symmetrical Bragg reflection, the imaginary part  $T''_{\infty y}$  can be represented in a similar way,  $T''_{\infty y}(z_s, z_{s'}) = V(z_s) - V(z_{s'})$ , where

$$V(z) = - \sum_\alpha \rho_\alpha \int_{-\infty}^{\infty} dx \sin(\mathbf{Q} \cdot \mathbf{u}_\alpha(x, z)). \quad (26)$$

The displacement component  $u_z^{(x)}$  decreases as  $1/x^2$  at large  $x$ , and the integral converges. Let us make an unphysical assumption for a moment, postulating that the product  $\mathbf{Q} \cdot \mathbf{u}_\alpha$  is always small in comparison with unity. This assumption implies that the misfit is dissolved in infinitesimal dislocations whose Burgers vectors are much smaller than the lattice spacing. Then the integrand of Eq. (26) can be expanded up to the term linear over  $\mathbf{Q} \cdot \mathbf{u}_\alpha$ , and the integration yields  $V(z) = q_{0z} z$ , where  $q_{0z}$  is given by Eq. (10). Substituting this expression into Eq. (23), one finds that the peak of the coherent intensity is located at  $q_z = q_{0z}$ , the position given by the mean distortions. However, this result is based on an unphysical assumption. The product  $\mathbf{Q} \cdot \mathbf{u}_\alpha$  can be of the order of unity,  $V(z)$  is smaller than  $q_{0z} z$ , and thus the shift of the coherent peak due to the misfit dislocations is smaller than  $q_{0z}$ .

The coherent intensity  $I_{\text{coh}}(q_z)$  calculated by Eq. (23) in the symmetrical 004 Bragg reflection is presented in Fig. 5. The peak width is given by the reciprocal thickness of the layer  $d^{-1}$ , and does not depend on the dislocation density. As the dislocation density increases, the peak intensity exponentially decreases, and the peak shifts. The shift of the coherent peak is smaller than the value (10) given by the mean distortions, which is shown in Fig. 5(b) by crosses. It is usually assumed, without any proof (see, e.g., Ref. 12), that positions of the diffraction peaks follow the mean distortions in the crystal. We showed in Sec. III that this statement is correct when the dislocation density is large. In that case, the peak is diffuse, and is governed by correlations of displacements at closely spaced lattice sites, i.e., by the mean local distortions in the crystal. The coherent peak observed at low dislocation densities is due to correlations between displacements at the sites separated by large distances. When the relative displacement is as large as the lattice spacing, it has no effect on the peak position, but makes a large contribution to the mean distortion. As a result, the shift of the coherent peak due to the misfit dislocations is smaller than the value given by the mean distortions.

The Debye-Waller factor (25) and the phase factor (26) can also be applied for the calculation of rocking curves under dynamical diffraction conditions, by employing them in the Takagi-Taupin equations. It is worth noting, however, that these factors describe the effect of the dislocations perpendicular to the incidence plane. The dislocations parallel to the incidence plane produce displacements which do not depend on the lateral coordinate  $x$  in that plane, but depend on the coordinate  $y$  normal to it. Then the solution of the dy-

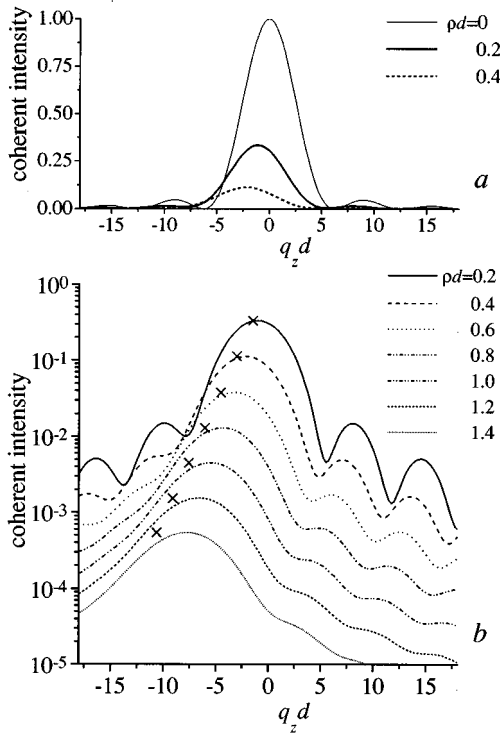


FIG. 5. Intensity of the coherent peak, Eq. (23), in the symmetrical 004 reflection presented on linear (a) and logarithmic (b) scales. The crosses mark positions of the peak maxima given by the mean distortions.

namical problem involves numerical integration of the Takagi-Taupin equations in each scattering plane with subsequent average of the intensities. The corresponding average in the framework of the kinematical theory is given by Eq. (3).

In an asymmetrical reflection, the integral (26) diverges logarithmically, due to the contribution of the displacement  $u_x^{(x)}$  which decreases as  $1/x$  at large  $x$ . The difference  $V(z_s) - V(z_{s'})$  converges, however. The imaginary part of the limit  $T''_{\infty y}$  can be written as a difference  $T''_{\infty y}(z_s, z_{s'}) = \tilde{V}(z_s) - \tilde{V}(z_{s'})$  of two finite quantities, to define

$$\tilde{V}(z) = - \sum_{\alpha} \rho_{\alpha} \int_{-\infty}^{\infty} dx [\sin(\mathbf{Q} \cdot \mathbf{u}_{\alpha}(x, z)) - v(x)]. \quad (27)$$

Here  $v(x)$  is an arbitrary regular function possessing the same asymptotic behavior on  $x \rightarrow \infty$  as the product  $Q_x u_x^{(x)}$  namely,  $Q_x u_x^{(x)} \sim 2Q_x b_x d / (\pi x)$ . We use the function  $v(x) = (2Q_x b_x / \pi) x d / (x^2 + d^2)$ . The integral  $\int_{-\infty}^{\infty} dx' [v(x') - v(x' - x)]$  is zero for large but finite  $x$ . This result is applied in Eq. (23), and means that the coherent peak does not shift in the  $q_x$  direction but remains in the same position as for the strained dislocation-free reference layer. Note that the unphysical assumption of dislocations with infinitesimal Burgers vectors would lead, in the same way as above, to the displacement of the Bragg peak by  $q_{0x}$ , Eq. (10), as given by the mean distortions.

The common treatment of the lateral position of the peak<sup>12</sup> is based on a consideration of the mean strain in the

layer which adopts additional atomic planes (the dislocation half-planes), while its length remains fixed. The uniform strain would give rise to a layer incommensurate with the substrate, a state which is never observed in the epitaxial growth. The state which is realized is essentially nonuniform, with strains concentrated at the misfit dislocations. At the dislocation, the displacement jumps by the Burgers vector. Considering the mean distortions, one uniformly dissolves the jumps among all atomic planes, and the mean strain effect is treated to cause a shift of the diffraction peak. However, the Burgers vector is equal to a lattice translation. An insertion of the dislocation extra half-plane does not directly influence the x-ray diffraction, but causes nonuniform distortions around the dislocation, which decrease as the distance from the dislocation increases. The mean effect of the elastic distortions is calculated above. The displacements decrease fast enough and do not change the mean lattice spacing. Thus, when the mean distance between dislocations exceeds the layer thickness, the layer contains slightly distorted regions between dislocations which give rise to the coherent Bragg peak, laterally unshifted with respect to the substrate peak. The strongly distorted regions around the dislocations cause diffuse scattering, whose peak position does not coincide with that of the coherent peak. As the dislocation density increases, the coherent peak intensity exponentially decreases, while the diffuse peak reaches the position given by the mean distortions.

Calculation of the diffuse intensity is considerably simplified in the limit of very small dislocation densities,  $\rho d \ll 1$ . In that case, the correlation function  $T(x, z_s, z_{s'})$  is small, and the expansion  $\exp(-T) \approx 1 - T$  can be applied in Eq. (24). Changing the sequence of the integrations, one receives, for  $q_x \neq 0$ ,

$$I_{\text{diff}}(q_x, q_z) = \sum_{\alpha} \rho_{\alpha} \left| \int_{-\infty}^{\infty} dx \int_0^d dz e^{iq_x x + iq_z z} \times [e^{i\mathbf{Q} \cdot \mathbf{u}_{\alpha}(x, z)} - 1] \right|^2. \quad (28)$$

In this limiting case, the dislocations perpendicular to the incidence plane contribute to the diffuse intensity additively, and the intensity is proportional to their density. The dislocations parallel to the incidence plane do not contribute to the diffuse scattering. Figure 6 presents distributions of the diffuse intensity calculated by Eq. (28). In the symmetrical Bragg reflection (Fig. 6, left column), the main spot of the diffuse intensity is elongated in the  $q_z$  direction, normal to the layer surface. It is accompanied by two satellite spots of lower intensity extending in the  $q_x$  direction [see Figs. 6(a) and 6(c)]. Comparing contributions of different types of the dislocations to sum (28), we found that each satellite is due to  $60^\circ$  dislocations with a definite tilt component  $b_z$  of the Burgers vector. Dislocations with opposite tilt components give rise to different satellites. These satellites are absent for edge dislocations (not presented). The satellites in the  $q_z$ -direction in Figs. 6(b) and 6(c) are the layer truncation effect. In the asymmetrical reflection (Fig. 6, right column), the diffuse spot is extended in two directions, perpendicular to the surface and perpendicular to the diffraction vector. The

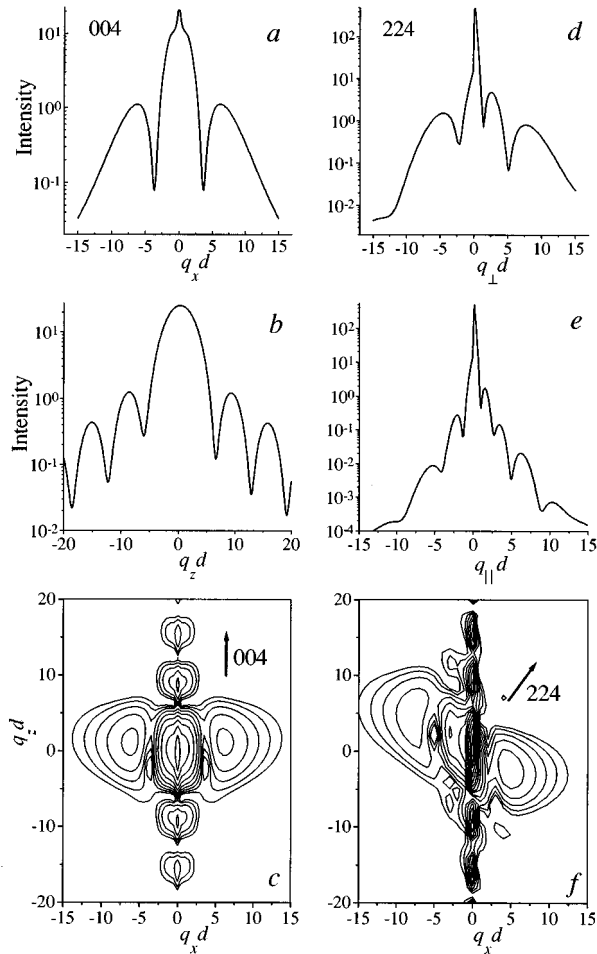


FIG. 6. Calculated diffuse intensities for small dislocation densities,  $\rho d \ll 1$ , of  $60^\circ$  misfit dislocations in the scans along the diffraction vector (a) and (d) and perpendicular to it (b) and (e), and the reciprocal space maps (c) and (f) in the symmetrical 004 Bragg reflection (left) and asymmetrical 224 reflection (right). The intensity changes between isointensity contours by a factor of 2.

scans along and perpendicular to the diffraction vector are asymmetric, and possess complicated structure with several satellites.

The transformation of the diffuse intensity distribution with increasing dislocation density is shown in Figs. 7 and 8. Calculations were performed on the basis of Eq. (24). Figure 7 presents scans of the intensity in the  $q_x$  and  $q_z$  directions, which correspond to the  $\omega$  and  $\omega/2\theta$  scans in the experiment, in the symmetrical 004 Bragg reflection. The  $q_z$  scan [Fig. 7(a)] demonstrates a continuous shift of the diffuse peak in the direction of the diffraction vector, when the dislocation density increases. At low dislocation densities, the shift is slightly smaller than the value (10) given by the mean distortions, but practically reaches this value at  $\rho d > 1$ . The width of the peaks is determined by the reciprocal thickness of the layer,  $\Delta q_z \approx 2\pi/d$ . Figures 7(b) and 7(d) present  $q_x$  scans of the peaks. Two satellites, which are clearly separated from the main part of the diffuse peak at very low dislocation densities [Fig. 6(a)], transform to “shoulders” of the peak. At dislocation densities  $\rho d > 1$ , the peaks become Gaussian-like ones. The transformation of the reciprocal

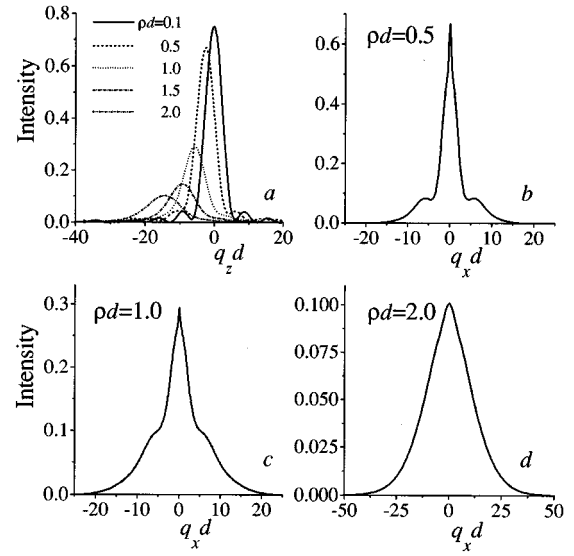


FIG. 7. Scans of the diffuse intensity in directions along (a) and perpendicular (b)–(d) to the diffraction vector for dislocation densities  $\rho d = 0.5$  (b), 1.0 (c), and 2.0 (d). 004 reflection.

space maps is shown in Fig. 8. As the dislocation density increases, the diffuse spots extend in a direction perpendicular to the diffraction vector, thus receiving the shape characteristic of large dislocation densities, cf. Figs. 2 and 3. In the asymmetric reflection, the peak shifts both laterally and normally to the layer. Let us remind the reader that the peak of coherent scattering  $I_{\text{coh}}(q_z)$  is located at  $q_x = 0$ . The positions of the coherent and diffuse peaks in the asymmetric reflection do not coincide, and represent a doublet. Such a doublet can be observed in a limited range of the dislocation densities, since the coherent intensity exponentially decreases with increasing dislocation density. At  $\rho d > 1$ , the position of the diffuse peak follows the mean distortions (10).

Separation of the coherent and the diffuse components of the scattered intensity in Eq. (22) implies infinitely good resolution of the measurements, allowing us to distinguish a sharp diffuse peak from the infinitely sharp  $\delta$ -shaped coherent peak. The effect of the instrumental resolution can be directly included into the calculations. The intensity  $\mathcal{I}(q_x, q_z)$  measured in the experiment is the convolution of the intensity  $I(q_x, q_z)$  due to the ideal plane wave illumination with the resolution function  $R(q_x, q_z)$ ,

$$\mathcal{I}(q_x, q_z) = \int \int dq'_x dq'_z I(q'_x, q'_z) R(q_x - q'_x, q_z - q'_z). \quad (29)$$

Expressing the intensity  $I(q_x, q_z)$  via the correlation function, Eq. (1), and calculating the convolution integral, one receives

$$\mathcal{I}(q_x, q_z) = \int_{-\infty}^{\infty} dx \int_0^d \int_0^d dz_s dz_{s'} e^{iq_x x + iq_z(z_s - z_{s'})} \times G(x, z_s, z_{s'}) R(x, z_s - z_{s'}), \quad (30)$$

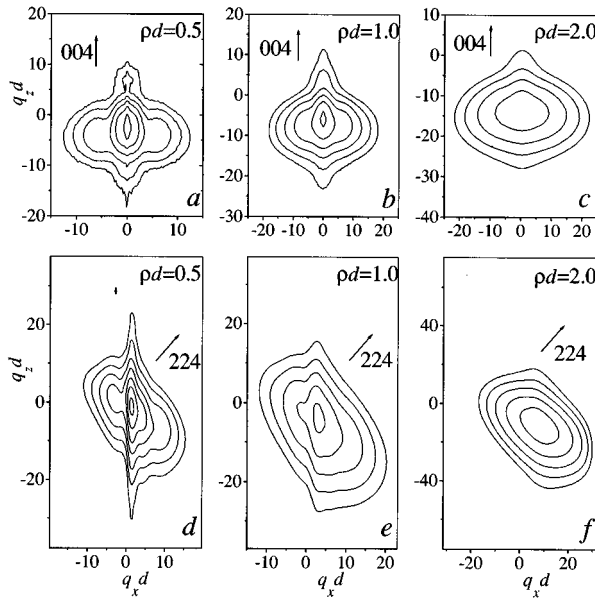


FIG. 8. Calculated reciprocal space maps of the diffuse intensity in the symmetrical 004 Bragg reflection (a)–(c) and asymmetrical 224 reflection (d)–(f) for dislocation densities  $\rho d = 0.5$  (a) and (d), 1.0 (b) and (e), and 2.0 (c) and (f). The intensity changes between iso-intensity contours by a factor of 2.

where  $R(x, z)$  is the Fourier transform of the resolution function  $R(q_x, q_z)$ . Equation (30) does not contain a  $\delta$ -function term, since  $R(x, z_s - z_s') \rightarrow 0$  as  $x \rightarrow \infty$ .

## V. EXPERIMENTAL RESULTS

The heteroepitaxial structures for the experimental study were chosen to cover a wide range of dislocation densities. In the results presented below, the parameter  $\rho d$  varies in the range from 0.1 to 500. That can be achieved only with different heteroepitaxial systems, by varying the mismatch and layer thicknesses. The results are presented in the order of increasing dislocation density. We describe the experimental setup first. The information concerning the heteroepitaxial systems is presented together with the corresponding x-ray-diffraction data.

The x-ray-diffraction measurements were performed with a triple-crystal x-ray diffractometer using  $\text{Cu } K\alpha_1$  radiation. A four-reflection Bartels-type monochromator provides a highly monochromatic x-ray beam ( $\Delta\lambda/\lambda = 1.3 \cdot 10^{-4}$ ) with an angular spread of less than 0.06 mrad. The direction of the incident beam with respect to the sample surface is changed by rocking the sample (angle  $\omega$ ), whereas the direction of the diffracted beam can be measured with an analyzer crystal in front of the detector (angle  $2\theta$ ). By tuning these two angles a reciprocal space mapping can be performed with a resolution  $\Delta Q/Q = 10^{-4}$ .

An initial stage of relaxation of an AlAs layer on a GaAs substrate provided us with a system of very low dislocation density. The 1.5- $\mu\text{m}$ -thick AlAs layer was grown by molecular-beam epitaxy (MBE) on a low miscut semi-insulating GaAs substrate, and covered by 20 nm of GaAs. The growth temperature was 510 °C and the growth velocity was 0.46  $\mu\text{m/h}$ . The surface reconstruction during the

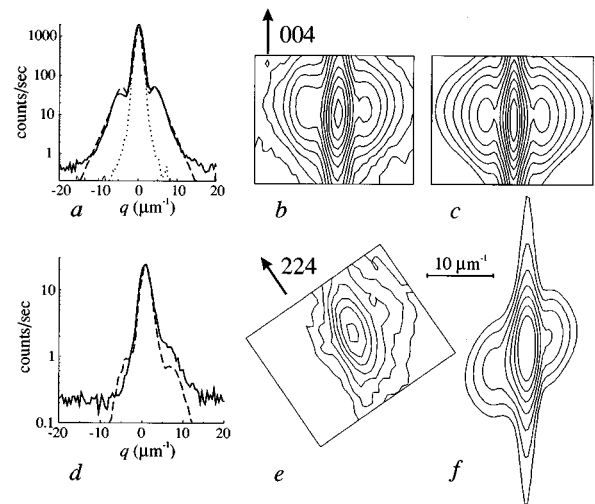


FIG. 9. Diffraction peaks for 004 (top) and 224 (bottom) reflections of a heteroepitaxial system AlAs/GaAs. The thickness of the AlAs layer is 1.5  $\mu\text{m}$ . Dislocation density  $\rho = 0.073 \mu\text{m}^{-1}$ , as measured by x-ray topography. (a) and (d) Scans along the diffraction vectors: measurements (full lines), simulations for uncorrelated uniformly distributed  $60^\circ$  dislocations (broken lines), and the resolution function measured with a GaAs sample (dotted line). (b)–(f) Reciprocal space maps: (b) and (e) measured and (c) and (f) simulated. The intensity changes between iso-intensity contours by a factor of 2.

growth of the AlAs was  $(2 \times 3)$ . The dislocation density  $\rho = 0.073 \mu\text{m}^{-1}$  was directly measured by x-ray topography, so that the product  $\rho d = 0.11$  was determined prior to the x-ray-diffractometry measurements. Measured and simulated scans of the peaks and the reciprocal space maps are compared on Fig. 9. The experimental resolution is comparable with the angular scale of the features of the diffuse scattering distribution, and the simulation was performed with the aid of Eq. (30), where the resolution function was taken as a Gaussian function with the half-width coinciding with that of the measured resolution function. In the symmetrical 004 Bragg reflection, Figs. 9(a)–9(c), the satellites of the peak are revealed. In the asymmetrical 224 Bragg reflection, Figs. 9(d)–9(f), the distribution of the diffuse intensity is asymmetric. The fine structure [cf. Fig. 6(d)] is not revealed, due to the resolution limitation. Measured and simulated intensity distributions are in a good agreement. We stress that simulations do not involve any fitting parameter. All parameters (dislocation density, layer thickness, angular resolution) were measured independently.

Figure 10 presents measured and simulated intensity distributions for another sample of the AlAs/GaAs heteroepitaxial system showing a higher dislocation density. The 3- $\mu\text{m}$ -thick AlAs layer was grown at essentially the same growth conditions as the previous sample. Only the growth velocity was slightly higher (0.57  $\mu\text{m/h}$ ). The relaxation of 22% was measured from the layer and substrate peak positions, which gives  $\rho d = 4.6$ . The peaks, Fig. 10, are close to anisotropic Gaussians, oriented perpendicularly to the corresponding diffraction vector. A good agreement between measured and simulated intensity distributions was found without any fitting parameter.

To reveal the satellite peaks of diffuse scattering at low

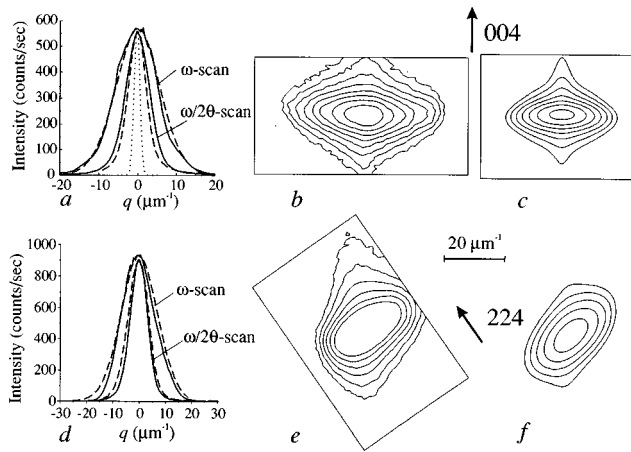


FIG. 10. Diffraction peaks for 004 (top) and 224 (bottom) reflections of a heteroepitaxial system AlAs/GaAs. The thickness of the AlAs layer is  $3 \mu\text{m}$ , the relaxation is 22%. Dislocation density  $\rho = 16 \mu\text{m}^{-1}$ . (a) and (d) Scans along and perpendicular to the diffraction vectors: measurements (full lines), simulations for uncorrelated uniformly distributed  $60^\circ$  dislocations (broken lines), and the resolution function measured with a GaAs sample (dotted line). (b)–(f) Reciprocal space maps: (b) and (e) measured and (c) and (f) simulated. The intensity changes between isointensity contours by a factor of 2.

dislocation densities separately from the central peak, the  $\text{Si}_{1-x}\text{Ge}_x/\text{Si}$  sample of a small layer thickness  $d = 0.12 \mu\text{m}$  was investigated. The layer was grown by low-pressure rapid thermal chemical vapor deposition (LP/RTCVD) at  $500^\circ\text{C}$  with  $x = 25\%$ . The measured reciprocal space maps, Figs. 11(b) and 11(d), are in a good agreement with the maps calculated for low dislocation densities, Figs. 6(c) and 6(f). The satellite peaks in the diffuse scattering pattern are revealed in both symmetrical and asymmetrical reflections. The measured and simulated intensity distributions in the  $\omega$  scans (perpendicularly to the diffraction vectors) are compared in Figs. 11(a) and 11(c). The angular distance between the satellite maxima on the simulated curve does not depend on the dislocation density, and occurs about 20% larger than the measured one. The discrepancy can be due to the elastic anisotropy, which was not taken into account in the simulations. Both coherent and diffuse components of the scattered intensity were included in the simulations [see Eq. (30)], and the dislocation density  $\rho = 1.25 \mu\text{m}^{-1}$  was determined from the value  $\rho d = 0.15$  found in the fit.

A  $\text{Si}_{1-x}\text{Ge}_x/\text{Si}$  sample grown by liquid phase epitaxy (LPE) was chosen as an example of a system possessing a larger dislocation density. During the growth (using an indium melt) the sample was cooled down from  $958$  to  $940^\circ\text{C}$ . The layer thickness  $5.5 \pm 0.5 \mu\text{m}$  was measured by scanning electron microscopy (SEM), the uncertainty is due to thickness variations over the sample. Figure 12 presents measured and calculated diffraction peaks for this  $\text{Si}_x\text{Ge}_{1-x}/\text{Si}$  system. The degree of relaxation measured from the relative peak positions of the layer and the substrate peaks is 98%. Using Vegard's law, an atomic concentration of the germanium in the layer of  $x = 4.3\%$  was calculated. The lattice mismatch is 0.18%, and the linear dislocation density  $\rho = 9 \mu\text{m}^{-1}$ , so that  $\rho d \approx 50$ . The layer peaks on the

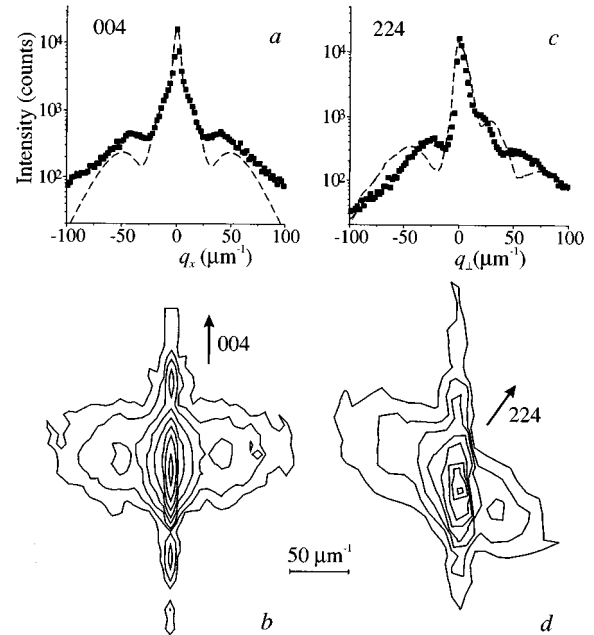


FIG. 11. Diffraction peaks for 004 (left column) and 224 (right column) reflections of a heteroepitaxial system  $\text{Si}_{1-x}\text{Ge}_x/\text{Si}$  ( $x = 25\%$ ). The layer thickness is  $0.12 \mu\text{m}$ . (a) and (c) Scans along the diffraction vectors: measurements (squares) and simulations for uncorrelated uniformly distributed  $60^\circ$  dislocations (broken lines). The dislocation density is taken in simulations  $\rho d = 0.15$ . (b) and (d) Measured reciprocal space maps.

reciprocal space maps measured in symmetrical and asymmetrical Bragg reflections, Fig. 12(b), are extended in the direction perpendicular to the corresponding diffraction vectors. The maps simulated in approximations (12) and (16), are in a good agreement with the measured ones. A more precise comparison of the measured and simulated peaks was performed in the scans along and perpendicular to the diffraction vectors, Fig. 12(a). In the scans along diffraction vectors ( $\omega/2\theta$  scan), the widths of the peaks calculated for uncorrelated  $60^\circ$  dislocations are in a good agreement with the observed peaks. However, in the scans along diffraction vectors ( $\omega$  scans), the observed peaks are broader in both symmetrical 004 and asymmetrical 224 reflections. The difference has been treated as a non-uniform tilt due to local variation of the difference  $\delta\rho = \rho_+ - \rho_-$  between densities of the dislocations with the opposite  $z$  components of the Burgers vectors. The mean variation  $\langle (\delta\rho/\rho)^2 \rangle^{1/2} = 0.12$  in Eq. (21) gives an agreement between the widths of the measured and the calculated peaks.

The AlSb/GaAs sample grown by molecular-beam epitaxy on a semi-insulating (001) GaAs substrate was chosen as an example of system with very large mismatch and accordingly large dislocation density. This sample contains a superlattice with 50 periods of 6 ML InAs and 6 ML AlSb (overall thickness  $0.2 \mu\text{m}$ ) on top of a  $1\text{-}\mu\text{m}$ -thick relaxed AlSb buffer layer. The growth temperatures for the buffer layer and the superlattice were  $570$  and  $425^\circ\text{C}$ , respectively. The AlSb layers were grown at  $1 \mu\text{m}/\text{h}$ , and the InAs layers at  $0.25 \mu\text{m}/\text{h}$ . The group-V-III beam flux ratio in both types of layers was 5:1. The superlattice is not relaxed with respect to the buffer layer.<sup>16</sup> The misfit of 7.9% between the GaAs

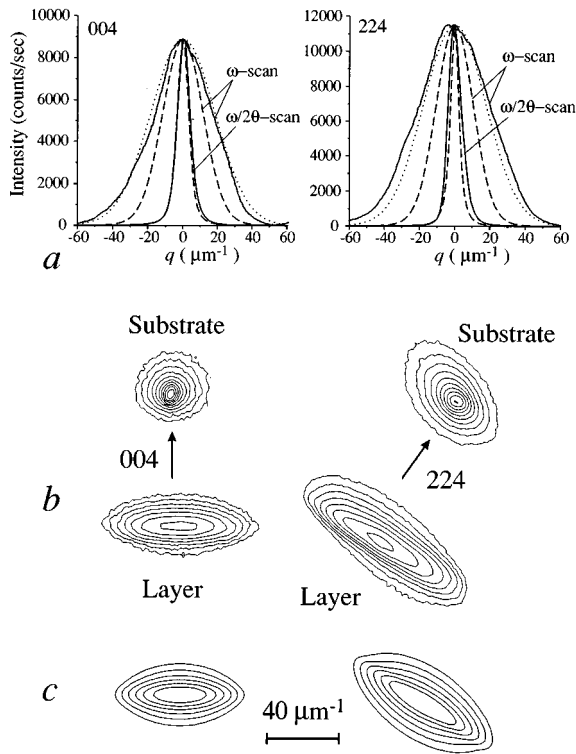


FIG. 12. Diffraction peaks for 004 and 224 reflections of the  $\text{Si}_{1-x}\text{Ge}_x/\text{Si}$  heteroepitaxial system ( $x=4.3\%$ ). (a) Scans along and perpendicular to the diffraction vectors: measurements (full lines), calculations for uncorrelated uniformly distributed  $60^\circ$  dislocations (broken lines), and taking into account the local tilt due to variation of the densities of dislocations with opposite  $z$  components of the Burgers vectors with  $\langle(\delta\rho/\rho)^2\rangle^{1/2}=0.12$  (dotted lines). (b) and (c): Measured and calculated (assuming uncorrelated uniformly distributed dislocations) reciprocal space maps. The intensity changes between iso-intensity contours by a factor of 2.

substrate and AlSb buffer layer, which is totally relaxed, gives rise to a linear density of the misfit dislocations  $\rho=400\ \mu\text{m}^{-1}$ , so that  $\rho d=480$ . A transmission-electron-microscopy (TEM) study reveals a complicated defect structure, including threading dislocations, microtwins and stacking faults (although this sample is the best in the series, No. 5 in Ref. 16). However, the densities of these defects are much smaller than the misfit dislocation density. For example, the mean distance between threading dislocations in the superlattice is about  $3\ \mu\text{m}$ , while the mean distance between the misfit dislocations is only  $2.5\ \text{nm}$ . The strain fields of the misfit dislocations give an evident mean effect, the relaxation, and the mean-square variation of these fields given by Eq. (15) provides the essential contribution to the peak width. The observed peaks, Fig. 13, are more than five times narrower than the ones calculated under assumption of uncorrelated dislocations. We conclude that the misfit dislocations are strongly positionally correlated, in agreement with the TEM observations of periodic arrays of misfit dislocations [cf. Fig. 7(c) in Ref. 16]. An agreement between measured and calculated peak widths can be achieved with the correlation parameter  $\gamma$  equal to 0.03.

The presence of the InAs/AlSb superlattice on top of the AlSb buffer layer provides us with the possibility to compare the strain variations in the layer with that in its upper part.

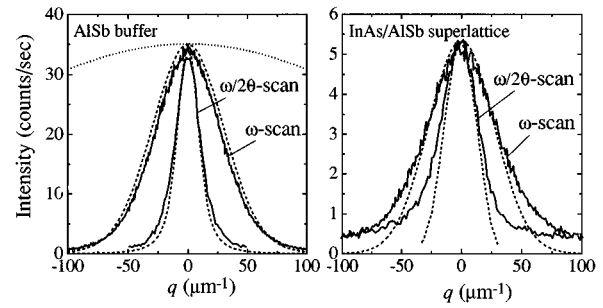


FIG. 13. Comparison between measured and calculated x-ray-diffraction peak profiles (004 reflection) of the InAs/AlSb superlattice (thickness  $0.2\ \mu\text{m}$ ) and the fully relaxed AlSb buffer layer (thickness  $1\ \mu\text{m}$ ) on a GaAs substrate. The measured intensity (full lines) agrees with the calculations for the correlation parameter  $\gamma=0.03$  (broken lines). The calculation of the  $\omega$  scan for uncorrelated dislocations (dotted line, buffer layer reflection) is shown for comparison.

The peak widths of the superlattice and the buffer layer are comparable, in agreement with the results of Sec. IIIB showing that the peak widths can be estimated from the distortions at the surface. Thus one can determine the nonuniformity of the strains at the top of the layer, caused by the misfit dislocations at its bottom interface, by just measuring the peak width of the layer. Approximations (12) and (16) are not sufficient to evaluate the superlattice peak profile along  $q_z$ , since they do not take into account the peak broadening due to the layer thickness. This profile was calculated by integration of Eq. (24), while for all other calculations presented in Figs. 12 and 13 approximations (12) and (16) are sufficiently accurate.

## VI. DISCUSSION

The problem considered in the present paper originates from the fact that the mismatch between the substrate and the layer possessing different lattice parameters is released by discrete portions, the dislocations, whose Burgers vectors are lattice translation vectors. A uniformly strained layer, which would be incommensurate to the substrate, is never realized in epitaxy. Having a pronounced mean effect, the lattice parameter relaxation, one can evaluate the mean-square effect due to nonuniformity of the strains concentrated at the dislocation lines. Comparison with the experimental results shows that in the case of large mismatch the observed peaks are narrower than follows from calculations for uncorrelated randomly distributed misfit dislocations. We explain the discrepancy by a spatial correlation of the dislocations.

Threading dislocations are frequently considered<sup>17-20</sup> as a main source of distortions causing broadening of the diffraction peaks. However, the mean distances between threading dislocations are reported to be of the order of  $1\ \mu\text{m}$ , comparable with the layer thickness, while the mean distances between the misfit dislocations in the same systems are more than two orders of magnitude smaller. As the calculations for uncorrelated misfit dislocations give peaks even broader than are observed, we restricted ourselves to the analysis of the misfit dislocations only and do not consider other defects which may give additional peak broadening. When the

threading dislocations contribute to the peak width, the degree of spatial correlations between the misfit dislocations has to be even higher than follows from the estimates below.

It was found in Sec. III B that the half-widths of the diffraction peaks at large densities of misfit dislocations are proportional to

$$\Delta q \sim Qb\sqrt{\rho/d}, \quad (31)$$

with a numerical factor depending on the orientations of the diffraction vector, the scan direction in the reciprocal space, Burgers vectors of the involved dislocations, etc. Proceeding to the angular units  $\omega_{\parallel} = \lambda q_{\parallel}/4\pi \cos\theta$  and  $\omega_{\perp} = \lambda q_{\perp}/4\pi \sin\theta$  for directions along and perpendicular to the diffraction vector (here  $\lambda$  is the x-ray wavelength and  $\theta$  is the Bragg angle), and keeping in mind that  $Q = (4\pi/\lambda)\sin\theta$  according to the Bragg law, one finds  $\omega_{\parallel} \sim \tan\theta$ , while  $\omega_{\perp}$  does not depend on the Bragg angle. The generic dependence  $\Delta q \sim Q$  does not refer to a particular type of defect, but is inherent for nonuniform strains. The same dependencies were found in the framework of the mosaic block model, with  $\omega_{\parallel}$  and  $\omega_{\perp}$  treated as due to the strain and the misorientation effects of randomly distributed dislocations.<sup>8,9,20</sup> In comparison, the finite size  $L_s$  of the sample or relevant blocks gives  $\Delta q \sim L_s^{-1}$  independent on the diffraction vector. The triple crystal measurements<sup>18,19</sup> show directly that  $\omega_{\parallel} \sim \tan\theta$  and  $\omega_{\perp}$  do not depend on the Bragg angle. (The double-crystal rocking curves give only a combination of  $\omega_{\parallel}$  and  $\omega_{\perp}$ .<sup>20</sup>)

Kyutt and co-workers<sup>18,19</sup> studied several heteroepitaxial systems with large mismatch. Comparing the measured peak widths of GaAs layers on silicon substrate with the calculations based on the results of Sec. III B, we find that the ratio of the simulated (for uncorrelated dislocations) to observed peak widths vary from 1 to 2, depending on the sample. For the GaSb/GaAs system, the widths of the peaks are similar to the results of present study for the AlSb/AlAs system, Fig. 13, and about 6 times narrower than calculated for the uncorrelated misfit dislocations. The discrepancy can be explained by spatial correlations of the dislocations, as discussed in Secs. III C and V.

Westwood *et al.*<sup>21</sup> investigated the  $\text{In}_x\text{Ga}_{1-x}\text{As}$  layers on GaAs, and found that the widths of double-crystal diffraction curves increase when  $x$  increases up to  $x \sim 0.5$ . A further decrease of the peak width at  $x > 0.5$  is accompanied by an increasing order in the network of misfit dislocations, observed by transmission electron microscopy. This behavior agrees well with the effect of spatial correlations of the misfit dislocations described in Sec. III C. It is worth noting, however, that the density of threading dislocations also decreases when  $x$  increases at  $x > 0.5$ . The effects of threading and misfit dislocations have not been resolved in the experiment.

The peak widths of partially relaxed  $\text{In GaAs/GaAs}$  multilayers observed by Rose and Pietsch<sup>22</sup> agree with the calculations for uncorrelated dislocations for small dislocation densities ( $\rho d \approx 1$ ). In almost relaxed systems ( $\rho d \approx 30$ ) the observed peaks are two times narrower, which can be explained with the correlation parameter  $\gamma = 0.25$ . This result also can be explained by the expected increase of the spatial correlations of dislocations with increased dislocation density.

Kidd, Fewster, and Andrew<sup>23</sup> investigated  $\text{In}_x\text{Ga}_{1-x}\text{As/GaAs}$  heteroepitaxial system with low dislocation densities,  $\rho d < 1$ . The observed reciprocal space maps agree with our Figs. 6, 8, and 11. The diffraction patterns contain two components; the Bragg peaks of the coherent scattering, whose intensity decreases with increasing dislocation density, and the diffuse spot. At low dislocation densities, the diffuse spot is extended along the diffraction vector and accompanied by the satellites in the  $q_x$  direction. The angular range between the intensity minima separating the central diffuse peak and the satellites of the 700-Å-thick sample, transformed to the dimensionless units used in the present paper, is  $\Delta q_x d \approx 6.5$ , to be compared with  $\Delta q_x d \approx 6.4$  derived from the experimental curve of our Fig. 11(a). A discrepancy with the value 7.4 which follows from the simulations, Figs. 6(a) and 11(a), can be due to elastic anisotropy, neglected in the simulations. It is worth noting that the 1400-Å-thick sample of Ref. 23 gives the value  $\Delta q_x d = 8.2$ , but the accuracy of its determination from the experimental data is lower.

Holý *et al.*<sup>24</sup> evaluated the scattering from misfit dislocations by treating the dislocation displacements  $\mathbf{u}(\mathbf{r})$  as Gaussian random variables, and representing the correlation function  $G(\mathbf{r}, \mathbf{r}') = \langle \exp\{i\mathbf{Q} \cdot [\mathbf{u}(\mathbf{r}) - \mathbf{u}(\mathbf{r}')] \} \rangle$  as  $\exp(-\frac{1}{2}\langle \{\mathbf{Q} \cdot [\mathbf{u}(\mathbf{r}) - \mathbf{u}(\mathbf{r}')] \}^2 \rangle)$ . As discussed in the Sec. I, such an approach is not generally valid, since dislocation displacements are not small and contain jumps by the Burgers vectors  $\mathbf{b}$  on the cuts. The result of further approximation,  $\mathbf{u}(\mathbf{r}) - \mathbf{u}(\mathbf{r}') \approx [(\mathbf{r} - \mathbf{r}') \cdot \nabla] \mathbf{u}(\mathbf{r})$ , coincides with our Eq. (11). The imaginary part of the correlation function (8) and the corresponding shift of the diffraction peak is missing, however. Note that the opposite sequence of approximations is correct for a crystal containing large dislocation densities with equal densities of dislocations with opposite Burgers vectors.<sup>25</sup> For small dislocation densities, the correct approach, discussed in Appendix A, is based on Poisson statistics. The spatial correlations of the dislocations can also be taken into account in this way. It is worth noting that the stress components presented in Ref. 24 give only strains, the symmetrical part of the distortion tensor, while integrals (9), (13), and (15) involve distortions. We use the displacement fields of the dislocation in half-space to determine the distortions, see Appendix B.

Häusler and Eberl<sup>26</sup> derived correlation function equivalent to Krivoglaz' for spatially uncorrelated dislocations, Eq. (A8), and applied it to simulations of the double-crystal rocking curves of partially relaxed  $\text{In}_x\text{Ga}_{1-x}\text{P/GaAs}$  heteroepitaxial systems. Their simulations are in good agreement with the observations indicating the absence of correlations in dislocation positions.

## VII. CONCLUSION

The lattice mismatch between the substrate and the epitaxial layer is relaxed by discrete portions, the dislocations. The nonuniformity of the strains concentrated at the dislocation lines gives rise to diffuse scattering. When the dislocation density is large, the diffraction peak from the layer is due to short-range correlations in positions of the atoms, and thus it is a diffuse peak. The intensity of the coherent peak reflecting the long-range correlations is exponentially small.

The position of the diffuse peak is governed by the mean distortions, and can be found without considering individual dislocations. The peak width is a mean-square effect due to nonuniformity of the strains, and depends on the Burgers vectors of individual dislocations. The peak shapes are close to anisotropic Gaussians extended in the direction perpendicular to the diffraction vector. The nonuniformity of the distortions in the topmost part of the layer is readily given by the peak half-width of the whole layer. The peak width for spatially uncorrelated dislocations is proportional to the square root of the dislocation density (see Fig. 4). Deviations of the observed peak widths from the calculated ones are due to correlations in the dislocation positions. The short-range correlations give rise to the peak narrowing, in comparison with the uncorrelated dislocations, by a factor of  $\sqrt{\langle(\Delta N)^2\rangle/N}$ , equal to the rms fluctuations of the dislocation number. The long-range nonuniformity of the dislocation distribution causes a broadening of the peak. Variation of the dislocation density broadens the peak of symmetrical Bragg reflection in the direction along the diffraction vector. Variation of the relative densities of the  $60^\circ$  dislocations with different tilt components of the Burgers vectors, while the total dislocation density is constant, broadens the peak in the tangential direction.

At low dislocation densities, the diffraction pattern contains both coherent and diffuse components. The intensity of the coherent peak decreases exponentially with increasing dislocation density. The position of the coherent peak does not follow the mean distortions. The shift of the peak in the direction normal to the surface is smaller than given by the mean distortions. The lateral shift is absent, despite the non-zero mean lateral strain. At very low dislocation densities, the diffuse scattering is extended along the diffraction vector and is accompanied by the satellites in direction perpendicular to the diffraction vector. As the dislocation density increases, the peak continuously transforms to an anisotropic Gaussian extended in a direction perpendicular to the diffraction vector.

Almost all features of the calculated diffraction patterns are confirmed experimentally. We observed satellites of the diffuse scattering peak at low dislocation densities, and the transformation of the peak to an anisotropic Gaussian with increasing dislocation density. At low dislocation densities, measured and simulated diffraction patterns are in good agreement. When all parameters are controlled independently, the simulations performed without any fitting parameter agree well with the experiment. At large dislocation densities, introduction of long- and short-range correlations in positions of the dislocations allows us to reach an agreement between measurements and simulations.

#### ACKNOWLEDGMENTS

The authors thank R. Hey and M. Hörické (Paul-Drude-Institut für Festkörperelektronik, Berlin) for the preparation of the AlAs/GaAs samples, P. Zaumseil and G. Fischer (Institut für Halbleiterphysik, Frankfurt/Oder) for the preparation of the LP/RTCVD SiGe/Si sample, E. Bauser and P. O. Hansson (Max-Planck-Institut für Festkörperforschung, Stuttgart) for the preparation of the SiGe/Si LPE sample, as well as B. Brar and H. Kroemer (University of California, Santa

Barbara) for the AlSb/GaAs sample. We also appreciate the help of U. Jahn (Paul-Drude-Institut für Festkörperelektronik, Berlin) and H. Raidt (Max-Planck Arbeitsgruppe ‘‘Röntgenbeugung,’’ Berlin) for performing the SEM measurements. We thank K. Häusler (Max-Planck-Institut für Festkörperforschung, Stuttgart) for helpful discussions. The work was supported by the German Bundesministerium für Forschung und Technologie (BMFT) under Contract No. 01 M 2929.

#### APPENDIX A: CORRELATION FUNCTION

In this appendix, we follow Ref. 11 to derive general expressions for intensity scattered by a crystal containing a random distribution of defects. In the framework of the kinematical approximation, the amplitude of the wave scattered by a crystalline object is proportional to the sum  $A(\mathbf{Q}) = \sum_s \exp[i\mathbf{Q} \cdot (\mathbf{R}_s + \mathbf{u}_s)]$  taken over all atoms of the crystal. Here  $\mathbf{R}_s$  is the position of  $s$ th atom in a defect-free reference crystal, and  $\mathbf{u}_s = \mathbf{u}(\mathbf{R}_s)$  is its displacement due to defects. The intensity  $I(\mathbf{Q}) = \langle |A(\mathbf{Q})|^2 \rangle$  is the result of the average over random positions of the defects. It can be presented as a double sum over all atoms,

$$I(\mathbf{Q}) = \sum_{s,s'} e^{i\mathbf{Q} \cdot (\mathbf{R}_s - \mathbf{R}_{s'})} G(\mathbf{R}_s, \mathbf{R}_{s'}), \quad (\text{A1})$$

where the correlation function is

$$G(\mathbf{R}_s, \mathbf{R}_{s'}) = \langle \exp[i\mathbf{Q} \cdot (\mathbf{u}_s - \mathbf{u}_{s'})] \rangle. \quad (\text{A2})$$

In a triple-crystal diffraction experiment, the beams are collimated in the incidence plane, while the acceptance window of the detector is large in the direction perpendicular to that plane. Taking the  $(Q_x, Q_z)$  plane as the incidence plane, we assume that integration of the intensity  $I(\mathbf{Q})$  over the  $Q_y$  component of the wave vector can be performed in the infinite limits. The integration of Eq. (A1) gives rise to the delta function  $\delta(R_{sy} - R_{s'y})$ , meaning that the two points  $\mathbf{R}_s$  and  $\mathbf{R}_{s'}$  lie in one and the same plane  $y = \text{const}$ . Thus the intensity can be represented as

$$I(Q_x, Q_z) = \sum_{s,s'}^{(y)} e^{i\mathbf{Q} \cdot (\mathbf{R}_s - \mathbf{R}_{s'})} G(\mathbf{R}_s, \mathbf{R}_{s'}), \quad (\text{A3})$$

where the superscript  $(y)$  at the sum indicates that  $(\mathbf{R}_s - \mathbf{R}_{s'})_y = 0$ , and the summation runs over the plane  $y = \text{const}$ .

To perform the statistical average  $\langle \rangle$ , one has to consider  $\mathbf{u}_s$  as a sum of contributions due to all defects of the crystal, and average over their random positions. Let us first consider the case when all defects produce displacements of one and the same type, i.e., defects differ only by their position, and then generalize the result to different types of defects. One can present the displacement of the  $s$ th atom as a sum over all defects  $\mathbf{u}_s = \sum_t \mathbf{u}_{st}$ , where  $\mathbf{u}_{st} \equiv \mathbf{u}(\mathbf{R}_s - \mathbf{R}_t)$  is the displacement at the position  $\mathbf{R}_s$  due to a defect in the position  $\mathbf{R}_t$ . The summation can be extended to all possible positions of the defects by introducing the occupation numbers  $c_t$  equal to 1 if a defect is present in position  $t$ , and 0 otherwise. The subscript  $t$  denotes positions which can be occupied by the defects, and its meaning depends on the type of the defects.

For straight dislocations lying in the plane of the interface, which are considered in the present paper, it counts the positions along the line in the plane of the interface perpendicular to the dislocation lines. Other general examples are straight dislocations in a bulk crystal, where possible positions are given by lattice points in the plane normal to dislocation lines, or dislocation loops, determined by positions of their centers. The mean value  $c = \langle c_t \rangle$  is the number density of the defects.

Thus one has  $\mathbf{u}_s = \sum_t c_t \mathbf{u}_{st}$ . Substituting this sum into Eq. (A2), one can present the exponential function as a product,

$$G(\mathbf{R}_s, \mathbf{R}_{s'}) = \left\langle \prod_t \exp[i c_t \mathbf{Q} \cdot (\mathbf{u}_{st} - \mathbf{u}_{s't})] \right\rangle. \quad (\text{A4})$$

Let us assume first that the defects are not correlated. Then Eq. (A4) contains a product of statistically independent terms. The average of each term is

$$\langle \exp[i c_t \mathbf{Q} \cdot (\mathbf{u}_{st} - \mathbf{u}_{s't})] \rangle = c \exp[i \mathbf{Q} \cdot (\mathbf{u}_{st} - \mathbf{u}_{s't})] + 1 - c, \quad (\text{A5})$$

since  $c_t$  takes on only two values, 1 with probability  $c$  and 0 with probability  $1 - c$ . One can rewrite Eq. (A4) as

$$\begin{aligned} G(\mathbf{R}_s, \mathbf{R}_{s'}) &= \prod_t \{ c \exp[i \mathbf{Q} \cdot (\mathbf{u}_{st} - \mathbf{u}_{s't})] + 1 - c \} \\ &= \exp \sum_t \ln \{ c \exp[i \mathbf{Q} \cdot (\mathbf{u}_{st} - \mathbf{u}_{s't})] + 1 - c \} \\ &\equiv \exp[-T(\mathbf{R}_s, \mathbf{R}_{s'})]. \end{aligned} \quad (\text{A6})$$

For small concentrations,  $c \ll 1$ , one can expand the logarithm to receive

$$T(\mathbf{R}_s, \mathbf{R}_{s'}) = c \sum_t \{ 1 - \exp[i \mathbf{Q} \cdot (\mathbf{u}_{st} - \mathbf{u}_{s't})] \}. \quad (\text{A7})$$

Generally, several types of defects producing different displacement fields contribute to  $\mathbf{u}_s$ . For example, one can consider inclusions of different sizes, dislocation loops of different orientations, straight dislocations of different line directions, etc., as different types of defects, and write the displacement as a sum  $\mathbf{u}_s = \sum_\alpha \mathbf{u}_{s\alpha}$  where the subscript  $\alpha$  counts defect types present in the crystal. In this paper, dislocations lying parallel or perpendicular to the incidence plane, as well as dislocations with the same line direction but differing by orientation of the Burgers vector, are considered as different types of defects. One can introduce occupation numbers  $c_{t\alpha}$  equal to 1 if the defect of type  $\alpha$  is present in position  $t$ , and 0 otherwise, and the number densities  $c_\alpha = \langle c_{t\alpha} \rangle$  of defects of type  $\alpha$ . Then Eq. (A7) is substituted for by

$$T(\mathbf{R}_s, \mathbf{R}_{s'}) = \sum_\alpha c_\alpha \sum_t \{ 1 - \exp[i \mathbf{Q} \cdot (\mathbf{u}_{st\alpha} - \mathbf{u}_{s't\alpha})] \}. \quad (\text{A8})$$

This correlation function is used in this paper.

Let us proceed now to the general case of spatially correlated defects, when the numbers  $c_{t\alpha}$  are statistically dependent. We start from the case of only one type of defect, and make use of the equality

$$\exp[i c_t \mathbf{Q} \cdot (\mathbf{u}_{st} - \mathbf{u}_{s't})] = 1 + c_t \{ \exp[i \mathbf{Q} \cdot (\mathbf{u}_{st} - \mathbf{u}_{s't})] - 1 \} \quad (\text{A9})$$

which is identically valid for both  $c_t = 0$  and 1. An effective way of evaluating the correlation function (A4) is to apply the Kubo cumulant expansion.<sup>11,27,28</sup> Instead of expanding product (A4) over the correlation functions  $\langle c_t c_{t'} \dots \rangle$ , one represents the x-ray correlation function as  $G(\mathbf{R}_s, \mathbf{R}_{s'}) = \exp[-T(\mathbf{R}_s, \mathbf{R}_{s'})]$  and expands  $T(\mathbf{R}_s, \mathbf{R}_{s'})$  over the correlation functions  $\langle (c_t - c)(c_{t'} - c) \dots \rangle$ .

The first term of the expansion depends on the mean concentration  $c$  and is given by Eqs. (A6) and (A7). The next term is expressed via the pair correlation function  $\langle (c_t - c)(c_{t'} - c) \rangle$ :

$$T^{(2)}(\mathbf{R}_s, \mathbf{R}_{s'}) = - \sum_{t < t'} \ln \left[ 1 + \frac{\Phi_t \Phi_{t'} \langle (c_t - c)(c_{t'} - c) \rangle}{(1 + c \Phi_t)(1 + c \Phi_{t'})} \right], \quad (\text{A10})$$

where  $\Phi_t = \exp[i \mathbf{Q} \cdot (\mathbf{u}_{st} - \mathbf{u}_{s't})] - 1$ . Further terms of the expansion become more bulky. The expansion can be simplified when the concentration  $c$  and also the correlations  $\langle (c_t - c)(c_{t'} - c) \dots \rangle$  are small. Retaining the terms linear over these quantities, one has

$$\begin{aligned} T(\mathbf{R}_s, \mathbf{R}_{s'}) &= - \sum_{l=1}^{\infty} \sum_{t_1 < t_2 < \dots < t_l} \Phi_{t_1} \Phi_{t_2} \dots \Phi_{t_l} \\ &\quad \times \langle (c_{t_1} - c) \dots (c_{t_l} - c) \rangle. \end{aligned} \quad (\text{A11})$$

Extension to cases of several types of defects is straightforward, and we present the first two terms only:

$$\begin{aligned} T(\mathbf{R}_s, \mathbf{R}_{s'}) &= - \sum_{t\alpha} c_\alpha \Phi_{t\alpha} - \frac{1}{2} \sum_{\alpha\alpha'} \sum_{t \neq t'} \varepsilon_{\alpha\alpha'}(\mathbf{R}_t - \mathbf{R}_{t'}) \\ &\quad \times \Phi_{t\alpha} \Phi_{t'\alpha'}, \end{aligned} \quad (\text{A12})$$

where  $\varepsilon_{\alpha\alpha'}(\mathbf{R}_t - \mathbf{R}_{t'}) = \langle (c_{t\alpha} - c_\alpha)(c_{t'\alpha'} - c_{\alpha'}) \rangle$  and  $\Phi_{t\alpha} = \exp[i \mathbf{Q} \cdot (\mathbf{u}_{st\alpha} - \mathbf{u}_{s't\alpha})] - 1$ .

The correlation function (A12) was applied in Sec. III C. As discussed in that section, when the correlation length of  $\varepsilon_{\alpha\alpha'}(\mathbf{R}_t - \mathbf{R}_{t'})$  is small compared with the length scale of the variation of the displacement fields, one can keep the terms  $\Phi_{t\alpha}$  constant during summation of  $\varepsilon_{\alpha\alpha'}(\mathbf{R}_t - \mathbf{R}_{t'})$ . Then the sums  $\varepsilon_{\alpha\alpha'} = \sum_{t \neq t'} \varepsilon_{\alpha\alpha'}(\mathbf{R}_t)$  are of special interest. These sums can be quite generally related to the mean square variation of the number of the defects.<sup>29</sup> Consider first defects of only one type. The correlation function  $\varepsilon(\mathbf{R}_t - \mathbf{R}_{t'}) = \langle (c_t - c)(c_{t'} - c) \rangle$  is defined for  $t \neq t'$ . The coinciding sites can be included in the summation (A12) by setting  $\varepsilon_{\alpha\alpha'}(0) = 0$ . On the other hand, one directly finds  $\langle (c_t - c)(c_t - c) \rangle = c(1 - c)$ , since  $\langle c_t^2 \rangle = \langle c_t \rangle = c$  for the bimodal spectrum of  $\{c_t\}$  consisting of 0 and 1. We restrict ourselves to small defect densities  $c \ll 1$ , and write

$$\langle (c_t - c)(c_{t'} - c) \rangle = \varepsilon(\mathbf{R}_t - \mathbf{R}_{t'}) + c \delta_{tt'}, \quad (\text{A13})$$

where  $\delta_{tt'}$  is the Kronecker's delta. Let us sum up the left- and right-hand sides of Eq. (A13) over  $t$  and  $t'$ . The sum  $\sum_t 1$  is equal to the number of the lattice sites on the summation interval, and  $c \sum_t 1 = N$  is the mean number of the defects on this interval. The sum  $\sum_t (c_t - c)$  is equal to  $\Delta N$ , the random variation of the number of defects on the interval. One has  $\sum_t \langle (c_t - c)(c_{t'} - c) \rangle = \langle (\Delta N)^2 \rangle$ , the mean-square variation of the number of the defects, and thus

$$\epsilon \equiv \sum_t \varepsilon(\mathbf{R}_t) = c \left( \frac{\langle (\Delta N)^2 \rangle}{N} - 1 \right). \quad (\text{A14})$$

The factor  $\gamma = 1 + c^{-1} \epsilon$ , employed in Sec. III C, is equal to  $\langle (\Delta N)^2 \rangle / N$ . When spatial correlations of the defects are absent, one has  $\langle (\Delta N)^2 \rangle = N$ , as in the ideal gas of noninteracting particles. In that limit,  $\epsilon = 0$  and  $\gamma = 1$ . The correlations of the defect positions decrease the fluctuations,  $\gamma < 1$ .

The generalization to several types of the defects is straightforward: one has, instead of Eq. (A13),

$$\langle (c_{t\alpha} - c)(c_{t'\alpha'} - c) \rangle = \varepsilon_{\alpha\alpha'} \langle \mathbf{R}_t - \mathbf{R}_{t'} \rangle + c_\alpha \delta_{\alpha\alpha'} \delta_{tt'} \quad (\text{A15})$$

and the summation over  $t$  and  $t'$  gives

$$\varepsilon_{\alpha\alpha'} \equiv \sum_t \varepsilon_{\alpha\alpha'} \langle \mathbf{R}_t \rangle = c_\alpha \left( \frac{\langle \Delta N_\alpha \Delta N_{\alpha'} \rangle}{N_\alpha} - \delta_{\alpha\alpha'} \right). \quad (\text{A16})$$

## APPENDIX B: DISPLACEMENTS DUE TO DISLOCATION PARALLEL TO SURFACE OF THE HALF-SPACE

Here, for the sake of completeness, we present the displacement due to a dislocation lying parallel to the surface of the isotropic half-space on a given distance  $d$  from it. This problem was first solved by Head<sup>13</sup> (see also Ref. 14). In the case of a screw dislocation, the condition of the stress-free surface is fulfilled by means of the image dislocation. In the case of an edge dislocation, the image dislocation compensates for only one component of the stress at the surface (the compressive stress, when the Burgers vector is perpendicular to the surface or shear stress when the Burgers vector is parallel to the surface). Thus the solution consists of three parts: displacement due to a dislocation in the infinite medium, the image dislocation, and an additional term.

We use the frame of Fig. 1 with the origin at the surface, the  $z$  axis is normal to the surface and the dislocation line is parallel to the  $y$  axis. The parameter  $\alpha = 1/[2(1-\nu)]$  is introduced, where  $\nu$  is the Poisson ratio.

The displacements due to an edge dislocation with the Burgers vector parallel to the surface  $\mathbf{b} = (b_x, 0, 0)$  consist of the dislocation displacements in the infinite medium,

$$u_{1x} = -\frac{b_x}{2\pi} \left[ \arctan \frac{z-d}{x} + \frac{\alpha x(z-d)}{x^2 + (z-d)^2} \right], \quad (\text{B1})$$

$$u_{1z} = \frac{b_x}{2\pi} \left[ \frac{1-\alpha}{2} \ln(x^2 + (z-d)^2) + \frac{\alpha x^2}{x^2 + (z-d)^2} \right], \quad (\text{B2})$$

the image dislocation

$$u_{2x} = \frac{b_x}{2\pi} \left[ \arctan \frac{z+d}{x} + \frac{\alpha x(z+d)}{x^2 + (z+d)^2} \right], \quad (\text{B3})$$

$$u_{2z} = -\frac{b_x}{2\pi} \left[ \frac{1-\alpha}{2} \ln(x^2 + (z+d)^2) + \frac{\alpha x^2}{x^2 + (z+d)^2} \right], \quad (\text{B4})$$

and the additional relaxation term

$$u_{3x} = \frac{b_x d}{\pi} \left[ \frac{(1-\alpha)x}{x^2 + (z+d)^2} - \frac{2\alpha x z(z+d)}{(x^2 + (z+d)^2)^2} \right], \quad (\text{B5})$$

$$u_{3z} = -\frac{b_x d}{\pi} \left[ \frac{z+d}{x^2 + (z+d)^2} + \frac{\alpha z((z+d)^2 - x^2)}{(x^2 + (z+d)^2)^2} \right]. \quad (\text{B6})$$

For an edge dislocation with the Burgers vector perpendicular to the surface  $\mathbf{b} = (0, 0, b_z)$ , the displacements due to a dislocation in the infinite medium are

$$u_{1x} = -\frac{b_z}{2\pi} \left[ \frac{1-\alpha}{2} \ln(x^2 + (z-d)^2) + \frac{\alpha(z-d)^2}{x^2 + (z-d)^2} \right], \quad (\text{B7})$$

$$u_{1z} = \frac{b_z}{2\pi} \left[ \arctan \frac{x}{z-d} + \frac{\alpha x(z-d)}{x^2 + (z-d)^2} \right], \quad (\text{B8})$$

the image dislocation gives

$$u_{2x} = \frac{b_z}{2\pi} \left[ \frac{1-\alpha}{2} \ln(x^2 + (z+d)^2) + \frac{\alpha(z+d)^2}{x^2 + (z+d)^2} \right], \quad (\text{B9})$$

$$u_{2z} = -\frac{b_z}{2\pi} \left[ \arctan \frac{x}{z+d} + \frac{\alpha x(z+d)}{x^2 + (z+d)^2} \right], \quad (\text{B10})$$

and the additional terms are

$$u_{3x} = -\frac{b_z d}{\pi} \left[ (1-\alpha) \frac{z+d}{x^2 + (z+d)^2} + \alpha \frac{2x^2 z + d(x^2 + (z+d)^2)}{(x^2 + (z+d)^2)^2} \right], \quad (\text{B11})$$

$$u_{3z} = -\frac{b_z d}{\pi} \left[ \frac{(1-\alpha)x}{x^2 + (z+d)^2} + \frac{2\alpha x z(z+d)}{(x^2 + (z+d)^2)^2} \right]. \quad (\text{B12})$$

The screw dislocation with the Burgers vector  $\mathbf{b} = (0, b_y, 0)$  has only one displacement component

$$u_{1y} = \frac{b_y}{2\pi} \arctan \frac{x}{z-d}, \quad (\text{B13})$$

and the image dislocation

$$u_{2y} = -\frac{b_y}{2\pi} \arctan \frac{x}{z+d} \quad (\text{B14})$$

provides zero stresses at the surface.

Using the displacements  $\mathbf{u} = \mathbf{u}_1 + \mathbf{u}_2 + \mathbf{u}_3$  for any component of the Burgers vector presented above, one finds that the stresses  $\sigma_{zz} \sim (1-\nu)(\partial u_z / \partial z) + \nu(\partial u_x / \partial x)$ ,  $\sigma_{xz} \sim (\partial u_x / \partial z) + (\partial u_z / \partial x)$  are equal to zero at the surface  $z=0$ .

- \*Permanent address: Institute of Crystallography, Russian Academy of Sciences, Leninskii pr. 59, 117333 Moscow, Russia.
- <sup>1</sup>A recent review of the different mechanisms of strain relaxation with special emphasis on the Si-Ge system can be found in MRS Bull. **21**, 4 (1996), with articles by A. Cullis (surface undulation), C. Roland (surface roughness), D. E. Jesson *et al.* (kinetics), and F. K. LeGoues (misfit dislocations).
  - <sup>2</sup>J. W. Matthews and A. E. Blakeslee, J. Cryst. Growth **32**, 265 (1976).
  - <sup>3</sup>Z. J. Radzinski, B. L. Jiang, G. A. Rozgonyi, T. P. Humphreys, N. Hamaguchi, and S. M. Bedair, J. Appl. Phys. **64**, 2328 (1988).
  - <sup>4</sup>D. H. Rich, T. George, W. T. Pike, J. Maserjian, F. J. Grunthaler, and A. Larsson, J. Appl. Phys. **72**, 5834 (1992).
  - <sup>5</sup>R. Köhler, Appl. Phys. A **58**, 149 (1994).
  - <sup>6</sup>P. F. Fewster, Semicond. Sci. Technol. **8**, 1915 (1993).
  - <sup>7</sup>A comprehensive set of experimental studies is presented in the special issue: J. Phys. D **28**, 4A (1995).
  - <sup>8</sup>P. Gay, P. B. Hirsch, and A. Kelly, Acta Metall. **1**, 315 (1953).
  - <sup>9</sup>M. J. Hordon and B. L. Averbach, Acta Metall. **9**, 237 (1961).
  - <sup>10</sup>M. A. Krivoglaz, Fiz. Met. Metalloved. **12**, 465 (1961).
  - <sup>11</sup>M. A. Krivoglaz, *X-Ray and Neutron Diffraction in Nonideal Crystals* (Springer, Berlin, 1996).
  - <sup>12</sup>S. N. G. Chu, A. T. Macrander, K. E. Stege, and W. D. Johnston, J. Appl. Phys. **57**, 249 (1985).
  - <sup>13</sup>A. K. Head, Proc. Phys. Soc. London Sect. B **66**, 793 (1953).
  - <sup>14</sup>J. Lothe, in *Elastic Strain Fields and Dislocation Mobility*, edited by V. L. Indenbom and J. Lothe (North-Holland, Amsterdam, 1992), p. 364.
  - <sup>15</sup>Y. Epelboin, M. Gandais, and C. Willaime, Phys. Status Solidi A **44**, 651 (1977).
  - <sup>16</sup>J. Spitzer, A. Höpner, M. Kuball, M. Cardona, B. Jenichen, H. Neuroth, B. Brar, and H. Kroemer, J. Appl. Phys. **77**, 811 (1995).
  - <sup>17</sup>V. Holý, J. Kubena, E. Abramof, K. Lischka, A. Pesek, and E. Koppensteiner, J. Appl. Phys. **74**, 1736 (1993).
  - <sup>18</sup>R. N. Kyutt, L. M. Sorokin, T. S. Argunova, and S. S. Ruvimov, Fiz. Tverd. Tela (Leningrad) **36**, 2700 (1994) [Phys. Solid State **36**, 1473 (1994)].
  - <sup>19</sup>R. N. Kyutt, S. S. Ruvimov, and T. S. Argunova, J. Appl. Crystallogr. **28**, 700 (1995).
  - <sup>20</sup>J. E. Ayers, J. Cryst. Growth **135**, 71 (1994).
  - <sup>21</sup>D. I. Westwood, D. A. Woolf, A. Vilà, and J. R. Morante, J. Appl. Phys. **74**, 1731 (1993).
  - <sup>22</sup>D. Rose and U. Pietsch, in *Strained Layer Epitaxy—Materials, Processing, and Device Applications*, edited by J. Bean, E. Fitzgerald, J. Hoyt, and K.-Y. Cheng, MRS Symposia Proceedings No. 379 (Materials Research Society, Pittsburgh, 1995), p. 251.
  - <sup>23</sup>P. Kidd, P. F. Fewster, and N. L. Andrew, J. Phys. D **28**, A133 (1995).
  - <sup>24</sup>V. Holý, J. H. Li, G. Bauer, F. Schäffler, and H.-J. Herzog, J. Appl. Phys. **78**, 5013 (1995).
  - <sup>25</sup>I. R. Peterson and V. M. Kaganer, Phys. Rev. Lett. **73**, 102 (1994).
  - <sup>26</sup>K. Häusler and K. Eberl (unpublished).
  - <sup>27</sup>R. Kubo, J. Phys. Soc. Jpn. **17**, 1100 (1962).
  - <sup>28</sup>S. Dietrich and W. Fenzl, Phys. Rev. B **39**, 8873 (1989).
  - <sup>29</sup>L. D. Landau and E. M. Lifshitz, *Statistical Physics* (Pergamon, Oxford, 1980).